Lappeenranta University of Technology
Faculty of Technology
Degree Programme in Technomathematics and Technical Physics

*Ekaterina Soboleva*

# ATOMIC FORCE MICROSCOPY INVESTIGATION OF NI PARTICLES DEPOSITED ON POROUS SILICON

Examiners: Professor Erkki Lähderanta
M. Sc. Pavel Geydt

## ABSTRACT

Lappeenranta University of Technology
Faculty of Technology
Degree Programme in Technomathematics and Technical Physics

Ekaterina Soboleva

**Atomic Force Microcopy investigation of Ni particles deposited on porous silicon**

Master's thesis

2015

60 pages, 37 figures and 6 tables

Examiners: Professor Erkki Lähderanta
M. Sc. Pavel Geydt

Keywords: porous silicon, surface modification, electro-chemical nickel deposition, AFM, KPFM, MFM

In this thesis properties and influence of modification techniques of porous silicon were studied by Atomic Force Microscope (AFM). This device permits to visualize the surface topography and to study properties of the samples on atomic scale, which was necessary for recent investigation. Samples of porous silicon were obtained by electrochemical etching. Nickel particles were deposited by two methods: electrochemical deposition and extracting from $NiCl_2$ ethanol solution. Sample growth was conducted in Saint-Petersburg State Electrotechnical University, LETI.

Kelvin probe force microscopy (KPFM) and Magnetic force microscopy (MFM) were utilized for detailed information about surface properties of the samples. Measurements showed the difference in morphology correlating with initial growth conditions. Submicron size particles were clearly visible on surfaces of the treated samples. Although their nature was not clarified due to limitations of AFM technique. It is expected that surfaces were covered by nanometer scale Ni particles, which can be verified by implication of RAMAN device.

**ACKNOWLEDGEMENTS**

It is my pleasure to thank Erkki Lähderanta for giving me opportunity to study at Lappeenranta University of Technology and to conduct an interesting research. I would like to thank my supervisor Ph. D. student Pavel Geydt for his comments, support and practical advices.

I am grateful to professor V. A. Moshnikov from department of Micro- and Nanoelectronics Technology in St. Petersburg State Electrotechnical University for advices and support.

Finally, I thank my relatives and friends for love, encouragement and patience during the time of writing this paper.

Lappeenranta, May 2015

Ekaterina Soboleva

**Table of contents**

**List of Abbreviations**

| | |
|---|---|
| P-Si | porous silicon |
| AFM | Atomic Force Microscopy; Atomic Force Microscope (device) |
| SPM | Scanning Probe Microscopy |
| KPFM | Kelvin Probe Force Microscopy |
| MFM | Magnetic Force Microscopy |
| SOI | silicon on isolator |
| FWHM | full width at half maximum |
| LED | light emitting diod |
| HF | hydro-fluoric acid |
| FB | feedback system |

## 1. Introduction

Development of porous nanostructures is one of the promising directions in Material Science. Obtaining of porous nanostructures is a promising direction in materials science [1, 2]. Porous silicon (P-Si) is a class of semiconductor materials whose properties highly depend on the production technology. P-Si was discovered in 1958, and initially it was considered as a side effect of polishing the silicon wafers at Bell Labs. In 1975, the technology of creating the insulating layers based on P-Si was developed. In 1990 Canham discovered P-Si photoluminescence in the visible range of the optical spectrum. This led to creation of detectors, filters, tunable mirrors etc. on recent decades [3 - 5].

P-Si is a material with a wide range of applications in electronics [3], microelectronics [4], photonics [5], functional electronics [6] and medicine [7]. It is used as material for electrodes of fuel cells and lithium-ion batteries among others. The internal structure of P-Si has a significantly developed surface, a system of channels and pores of different size ranges (system-related nano-, meso- and micropores).

Preparation of P-Si with a complex geometry of 3D-channels has a special interest for the industry in idea to create a wide range of devices in sensor technology, MEMS, nonlinear optics, medicine etc. Moreover, P-Si can be used as the matrix material where different functional inclusions can be introduced in the pores.

Besides the current flow during the etching, UV-illumination is one of the additional parameters of electrochemical anodization. For example, wavelength of the incident radiation, the illumination type (continuous, periodic) backlight region etc. can affect the result. Therefore, design possibilities of porous layer structure can be expanded. Moreover, illumination of Si substrate during electrochemical anodization allows forming vertically arranged regions with different characteristics of the porous structure in one Si layer. Hence, porosity can change inside the layer. Such P-Si layers, characterized by variative structure of the porous layer in the lateral direction, are of interest for experimental modeling of P-Si structures within a sample and permit to create waveguides, Bragg mirrors, interference filters, microcavities, fuel cell electrodes, micropumps etc.

Nowadays, a large number of works [8 - 11] are devoted to the study of forming [9, 10] and improving [8, 11] the properties of materials for functional nanoelectronics. One of

these methods is the surface modification. For example, various forms of carbon are introduced to increase the intensity of the photoluminescence of porous silicon [12]. Additionally, layering on matrix porous material is applied to increase the selectivity and sensitivity to gases.

Nickel is a technological material with whole range of applications in Nano Science. It is important material in nickel-containing batteries, as well as in a wide range of technological applications, including electrochromic devices, water electrolysis, electrosynthesis and fuel cells [13]. Nickel is also used to improve corrosion resistance and wear resistance, to prepare the surface for the application of enamels and organic coatings. Among other applications, nanocomposites containing nickel may be recalled. Such materials can exhibit specific magnetic properties and can increase the selectivity of gas-sensitive sensors [14]. Therefore, it is expected that nickel deposition on porous silicon can improve the gas sensing properties of porous silicon.

Due to the large differences in properties of Si and Ni materials, depending on the growth conditions, it is desired to study the process parameters to develope the technology of their formation. It is presumed to measure surface morphology, electrical and magnetic properties of such combined material. According to size of structures (nm) it is vital to use precise instruments, for example AFM.

Therefore, motivation of this work was to investigate the properties of nickel (Ni) particles deposited on P-Si by Atomic Force Microscopy (AFM). Second interest was to find capabilities of different SPM modes (e.g. AFM, KPFM, MFM) in such investigation. Moreover, the influence of creation process conditions on surface properties was studied. Finally, the interaction of the surface with Ni particles was clarified.

## 2. Theoretical part

Main characteristics, applications and preparation methods of porous silicon and its modifications are presented in this chapter. This information was important to know before the study. It helped in formulating the task and planning the experiment.

Porous silicon was produced from crystalline silicon. Silicon is one of the basic materials of solid-state electronics because of significant possibilities to control its characteristics. Its properties in the crystalline and amorphous phases are thorougly studied and can be found in almost all modern textbooks on solid state physics.

Silicon is a second abundant chemical element (after oxygen) on our planet. Despite the fact that pure silicon has chemical inertness under normal conditions, it is not existing on Earth, although it is about a quarter of the planet mass (approximately 28% of the mass of the Earth's crust). Most of silicon is distributed in the form of silica or silicon oxide (IV) $SiO_2$ (ocean and river sand, quartz etc.). Silicon dioxide shares about 12% of the mass of the Earth's crust and is part of hundreds of different natural silicates and aluminum silicates, while porous silicon is completely artificial material. Therefore, parameters of its growing conditions should be fully studied.

### 2.1. Porous silicon (P-Si). Main characteristics and applications

It is difficult to imagine electronics without silicon. Figure 1 presents the discovery progress of the porous silicon technology. Figure 2 shows the development of theories about this material. Later this information will be described in more detail.

In late 1950’s Uhlir and Turner first reported that silicon surface can be changed during anodization in HF solutions [1, 15, 16]. Later, Memming and Schwandt proposed another theory of this changings [2]. Firstly, scientists suggested that the film on silicon surface was grown during the anodic dissolution. Then they proposed that brown film was a dissolution product resulted from disproportionation reaction [1, 17]. The formation of etch pits and tunnels on silicon of n-type conductivity was reported in the early 1970's [1,18, 19]. By early 80's it was established that the brown films on silicon substrate are formed with the same single crystalline structure as the substrate [1, 20 - 24].

Many theories on the formation mechanisms of P-Si appeared since then. Beale et al. proposed that the material in the P-Si is depleted of carriers [1, 25]. Smith et al. suggested that diffusion of holes limits the rate of pore growth [1, 26 - 28]. Unagami postulated that

passive silicic acid is deposited on the pore walls and promotes the P-Si formation [1, 29]. Alternatively, Parkhutik et al. suggested that the P-Si formation is similar to that of porous alumina [1, 17].

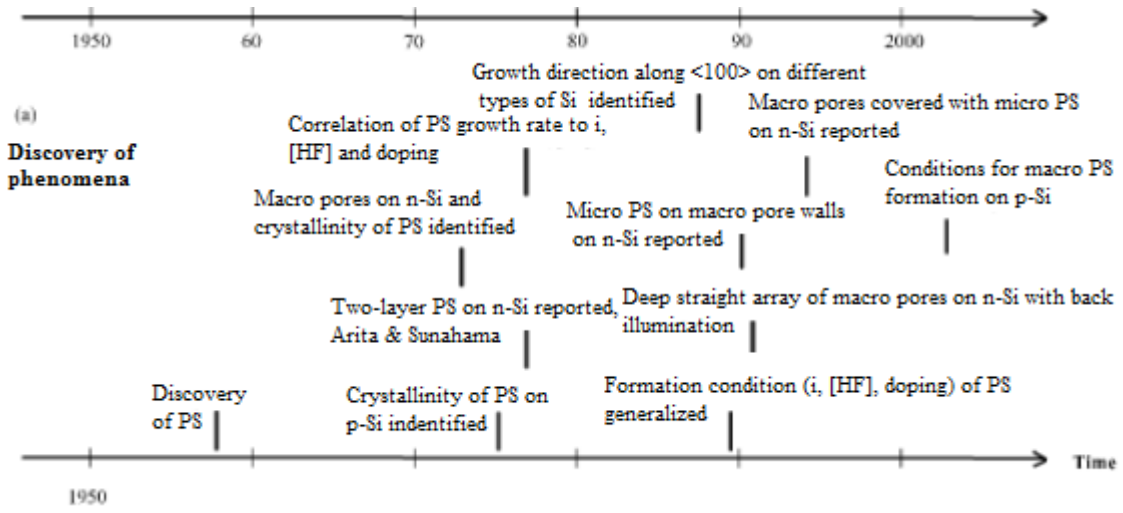


**Figure 1.** Progress in the discovery of morphological phenomena of porous silicon [1].

Zhang et al. established the conditions for P-Si formation on all types of substrates in terms of current density and HF concentrations by the end of 1980's. They assumed that P-Si formation by anodization depends on silicon electronic properties (doping type and concentration) and on the nature of electrochemical reactions [1, 31].

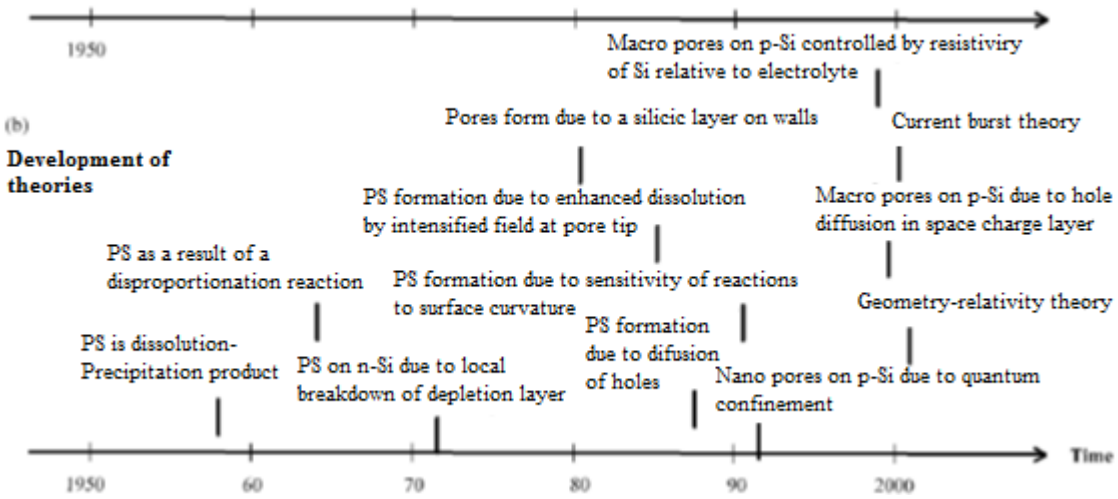


**Figure 2.** Progress in the development of theories on formation mechanism of porous silicon [1].

Lehmann and Foll reported the formation of straight, smooth and well-spaced macro pore arrays on n-Si [2]. It was done in early 1990's using backside illumination and surface patterning. They postulated that this phenomenon is determined by the relative rates of carrier transport in the silicon semiconductor and mass transport in the electrolyte. For the micro pores formed on p-Si a quantum confinement model was proposed by Lehmann and Gosele. Thus the pore walls are depleted of carriers and do not dissolve during the anodization. The surface curvature model was proposed at about the same time (by Zhang) [1, 32]. It postulated that the distribution of reaction on a curved pore bottom can be affected by surface curvature.

Another suggestion was the current burst theory [1, 33]. In the late 1990's, Foil et al. proposed that the electrochemical reactions operate in microscopic units. These reaction units have a temporal and a spatial distribution in number and in the state of activity. The synchronization of these operation units at certain time and geometrical scales provoke the pores formation.

Two-layer P-Si (micro P-Si on surface of a macro P-Si) formed on n-Si under front illumination had been reported in the late 70's [1, 20], but was only little investigated until the 90's. The micro P-Si may have a fractal-like geometry. Its structure can vary in the same layer as diameter (from a few nm to hundreds of nm). It was assumed that the mechanism of a macro P-Si formation under front illumination is the same as for the macro P-Si formation in the dark. According to Arita the amorphous-like P-Si is caused by the photo carriers generated in the depletion layer [3]. Alternatively, Clement et al. suggested that the macro P-Si shattering into filaments due to residual stress can be responsible for the micro P-Si formation under illumination [3].

Macro P-Si and two-layer P-Si formed on lowly doped p-Si in anhydrous organic HF solutions was first found by Propst and Kohl in the mid 1990's [3]. It was claimed to be related to the chemistry of organic solvents. Such P-Si type was later found to be formed in aqueous solutions also. It is not proved that walls of the macro pores will be covered by a micro P-Si layer. Wehrspohn et al. suggested that the formation of macro P-Si on lowly doped p-Si requires a higher resistivity of the substrate than that of electrolyte [1 - 3]. However, it was also found that macro P-Si can be formed in electrolysis that has much higher resistance than the silicon substrate. Alternatively, Lehmann and Ronnebeck

postulated that the macro P-Si formation on lowly doped p-Si is due to the effect of thermionic emission. It is more sensitive to barrier height rather than barrier width [2]. More recently, Zhang' proposed that this material is caused by the non-linear potential distribution in the highly resistive substrate [1, 35].

Some ideas have been elaborated with mathematical formulation. For example, a theoretical modeling attempted by Jaguiro et al [1, 44]. Most theories have considered only certain aspects of the complex morphology and formation of P-Si. Also, these theories did not take into account the many details of anodic electrochemical reactions and processes of the silicon electrolyte interface. However, a complete description of the morphological features of P-Si requires the integration of the all the morphological aspects. Any theory for the mechanisms of P-Si formation without this integration will be insufficient to explain morphological details [3].

Morphology is one of the main characteristics of P-Si. However, it is difficult to analyze this parameter because it is connected with wide variations in pore size, shape, orientation, interconnection and distribution. The most common characteristics are: density, porosity and pore size. Three types of densies are: true, bulk and apparent. The first one excludes pores and voids. The second one is the density of the material including every kind of pores (open, closed and inaccessible) and voids. The last one includes only closed and inaccessible pores.

According to IUPAC definition, porosity is the ratio of the total pore volume to the apparent volume [4]. Three types of porosies are also distinguished: open, closed and total. In the first case pores are accessible to a physical solid probe. Second type means the volume of pores inaccessible to the probe. Last one takes into consideration the volume of all pores of the material.

Among the morphological features pore diameter is the most commonly determined. According to the IUPAC standards three types of porous silicon exist. They are classified by the pores size [1-5]:

1) **Micropores.** The pores widths is smaller than 2 nm.
2) **Mesopores.** Pores have widths between 2 and 50 nm.
3) **Macropores.** Their widths is larger than 50 nm.

N.B. Pore size among meso- and micro- was found for samples in this work.

Equally important aspects are features such as pore orientation, fill of macro pores, branching and depth variation of a P-Si layer. Figures 3 - 6 briefly represent them. The pore growth is anisotropic process and depends on the substrate orientation and direction of carrier source. Their relative effect on the pores orientation is determined by the electrochemical reactions at the pore bottom (Figure 3). Figure 4 presents different types of pore branching. Individual pores can distribute straight in the "selected" direction with branching in dependence to the formation conditions. Figure 5 gives an explanation how macro pores can be filled with micro pores. Depth variation of P-Si layer can also vary from the surface to the bulk (Figure 6). There are two types of depth variations: 1) gradual change of pore diameter, where pore diameter is constant; and 2) abrupt change of pore diameter with a large difference in it (three orders of magnitude). The second type is also called two-layer P-Si (Figure 6, c) [1 – 5].

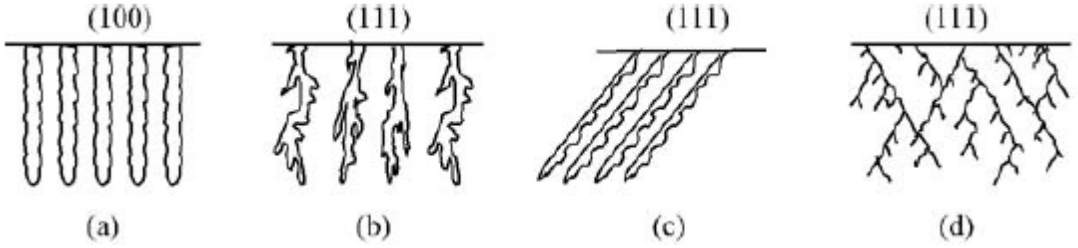


**Figure 3.** Pore orientation. (a) aligned to <100> and source of holes; (b) roughly aligned to source of holes; (c) partially aligned to <100> and source of holes and (d) aligned only to <100> [1].

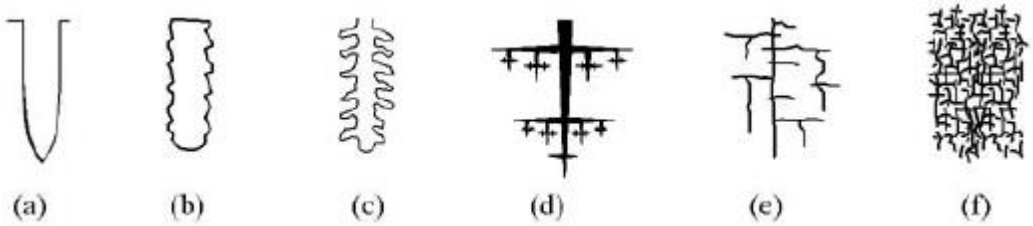


**Figure 4.** Branching. (a) smooth pore wall; (b) branches shorter than diameter; (c) second level branches; (d) dendritic branches; (e) main pores with second and third level branches; (f) dense, random and short branches [1].

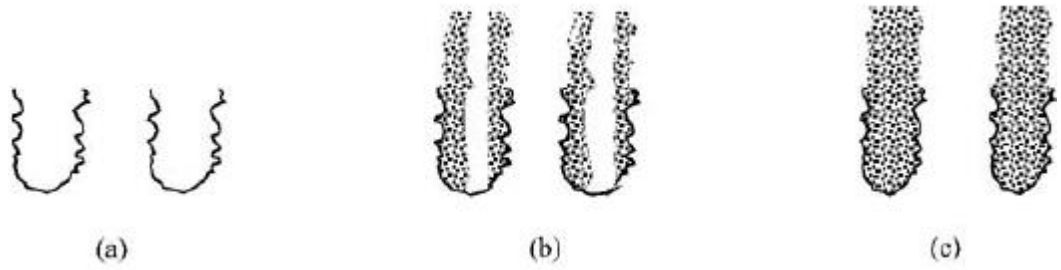


**Figure 5.** Filling of macro pores. (a) unfilled; (b) partially filled with micro pores; (c) fully filled [1].

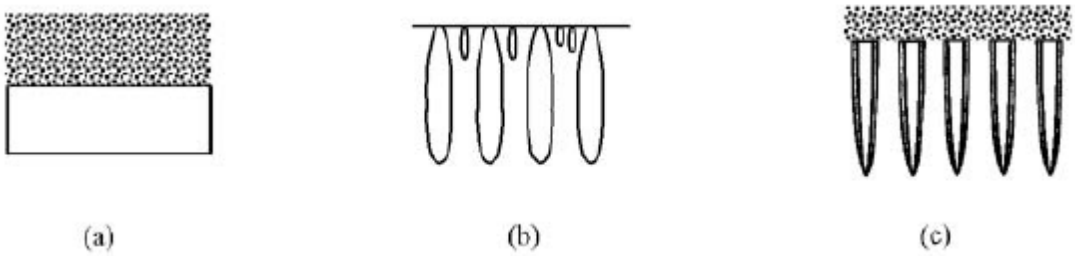


**Figure 6.** Depth variation of P-Si layer. (a) single porous layer; (b) macro porous layer with smaller pores near the surface; (c) micro porous layer on top of macro porous [1].

**Applications.** The porous silicon is dielectric material with a wide range of applications. They are presented in Table 1 [3]. P-Si properties which are used in each area are also shown. The P-Si usage also depends on its structure (pore diameter, the values of porosity, thickness of the porous layer etc.). Table 2 shows examples of various types of P-Si applications [4].

Distribution by application exist in dependence to pore size. P-Si was not used in production until the luminescent properties of microporous silicon were discovered. The first large-scale commercial product based on P-Si was silicon on isolator (SOI) wafers with usage of mesopores. Another application of mesoporous silicon in solar cells was proposed by Japanese and German groups. Utilization of mesoporous silicon allows to create thin solar cells with efficiencies up to 15% [5].

Occasionally it happens that mesopores are mentioned as micropores. In general, it may be linked with the usage of mesopores in areas of micropores. For example, sensors and sacrificial layers can be produced on mesoporous silicon. In some cases mesoporous structure is more preferable than microporous because of its better mechanical stability.

**Table 1.** Potential application areas of porous silicon [3].

| Application area | Role of porous silicon | Key property |
|---|---|---|
| Optoelectronics | LED | Efficient electroluminescence |
| | Waveguide | Tunability of refractive index |
| | Field emitter | Hot carrier emission |
| | Optical memory | Non-linear properties |
| Micro-optics | Fabry-Pérot Filters | Refractive index modulation |
| | Photonic bandgap structures | Regular macropore array |
| | All optical switching | Highly non-linear properties |
| Energy conversion | Antireflection coatings | Low refractive index |
| | Photo-electrochemical cells | Photocorrosion cells |
| Environmental monitoring | Gas sensing | Ambient sensitive properties |
| Microelectronics | Micro-capacitor | High specific surface area |
| | Insulator layer | High resistance |
| | Low-k material | Electrical properties |
| Wafer technology | Buffer layer in heteroepitaxy | Variable lattice parameter |
| | SOI wafers | High etching selectivity |
| Micromachining | Thick sacrificial layer | Highly controllable etching |
| Biotechnology | Tissue bonding | Tunablet chemical reactivity |
| | Biosensor | Enzyme immobilization |

Macropores can be used for such purposes as functional layers in microelectronics, antireflection coating, implants etc. [3, 4]. It can be possible due to its attractive features like large aspects ratios (length/diameter), possibility to define geometries, large porosities and thus large volume and full compatibility with Si technology. However, macropores utilization can have some difficulties, e.g. Si technology often needs an expensive infrastructure for research and development.

**Table 2.** Porous silicon application areas [4].

| Pores size | Application area | Key property |
|---|---|---|
| Micro-pores | Solid-state luminescent devices (light diodes, avalanche LEDs) | Photoluminescence |
| | Sensors adsorption type, humidity sensors (discrete, integral) | Great effective surface, and as a result high reactivity (with the possible modification of the P-Si surface by various active substances) |
| | Buffer layers for heteroepitaxy | The presence of pores, which can be mechanical relaxation of stresses arising at the interface layer-substrate |
| Mezo-pores | The functional layers in ICs, SOI structure | Great effective surface, and as a result high reactivity |
| | Antireflection coating (solar cells) | Significantly developed surface morphology, low reflectivity |
| | Integral resistors relatively high denominations (more than 1 MOhm / square) | P-Si oxidized to SiO2 due to its high reactivity becomes an insulator |
| | Implants, biosensors, immobilization of enzymes | Biocompatibility, significantly developed surface morphology |
| Macro pores | Photonic crystals | Strictly ordered structure of P-Si |
| | MEMS | The presence of pores, a large effective surface area, the change in electrical properties relative to the substrate Si |
| | Matrix materials | The presence of pores of different configurations |
| | Fuel cells electrodes | The presence of pores of different configurations, great effective surface |
| Various structure | Waveguides, Bragg mirrors, Fabry-Perot filters, microcavities | Different refractive index in layers with different porosity and pore diameter |

Three fields in macroporous silicon applications can be distinguished: microelectronic and mechanical systems (MEMS), optics and "surface". The last one means the usage of large surface to volume ratios [5].

Porous silicon is a material for fabrication of multilayers such as Distributed Bragg Reflectors. It is possible because the refractive index and thickness of the layers can be selected by changing the formation parameters during the fabrication process.

P-Si with microcavity structure can be used as band-pass filters, tunable mirrors and detectors. This structure can reduce the full width at half maximum (FWHM) in cases of photoluminescence and electroluminescence applications. Although waveguides based on multilayers are not widely reported they attract a great interest. These devices have different guiding mechanism and they can be used to confine, manipulate and guide the photons [3].

P-Si multilayers can be used for sensing different substances, i.e. hydrocarbon sensors and biosensors. In these devices the optical properties of P-Si microcavities are analyzed. Another type of sensors are humidity detectors based on study of electrical properties. For instance, a capacitive sensor based on mesoporous silicon for detection of polar solvents (ethanol, methanol acetone chloroform) and non-polar organic solvents (toluene) is described in [6, 8]. Authors of [6] analyzed the electrical properties of devices (impedance). Another examples are the works [7, 9], where detection of biomolecules like glucose, DNA, immunoglobulins, bacteria, viruses, triglycerides, phenolics, organophosphates, warfare agents and cancer were thoroughly studied and incited. Authors of [10] suggested that researchers are trying to improve the design and sensing schemes for optical and electrical-based sensors. The most important parameters are fast response time, sensitivity, selectivity and stability [10].

Another area of P-Si application is fabrication of electroluminescent devices like light emitting diodes (LEDs) or injection lasers. Also, photodetectors can be based on P-Si multilayers. This material can be used as anti-reflecting coating in solar cells. P-Si may be applied as sacrificial layer in micromachining due to its ability to dissolve [3].

The latest trend in the research and usage of porous silicon is a drug delivery. For example, in [11] porous silicon is described as an attractive material for controlled drug delivery applications to treat cancer.

## 2.2. Preparation of P-Si

This part will discuss the most common method for porous silicon creation. It is known, that porous silicon is the material which properties and the parameters depend on the methods and conditions of preparation. Thus, the methods and their impact on the structure and properties of the material will be considered.

### 2.2.1. Etching

In the earliest works on porous silicon, it is mainly obtained by electrochemical anodization. This method is known also as electrochemical dissolution of silicon wafers in solution of hydrofluoric acid (HF) or etching. Every process has its own parameters that can influence its formation and morphology. For etching they are:

- The substrate doping
- The current density
- The etching time
- The solution composition (including the HF concentration)
- The illumination during the etch (predominantly for n-type Si).

Table 3 briefly explains the influence of some anodization parameters on porosity, etch rate and critical current. This table shows the consequence of one parameter increasing while others are staying without changing. For instance, if one increases the HF concentration, then the porosity will decrease, however, other parameters remain the same [3].

Electrolytes for the anodic electro-chemical etching of silicon are divided into several types.

1. “Aqueous-electrolytes” (abbreviated with “aqu”). They derived from the $HF–H_2O$ system and include not only all mixtures of HF (commonly 49% p.w.) with water, but also fluorine bearing salts (e.g. $NH_4F$), additions of ethanol ($C_2H_4OH$) and/or acetic acid ($CH_3COOH$). The nominal concentration of F may range from 0.001 to 49%.

They have a ‘‘PSL-peak’’ in the I(V)-characteristics and they are tend to form $SiO_2$ (see Figure 7).

**Table 3.** Effect of anodization parameters on porous silicon formation [3].

| | Porosity | Etch rate | Critical current |
|---|---|---|---|
| HF concentration | *decreases* | *decreases* | *increases* |
| Current density | *increases* | *increases* | - |
| Anodization time | *increases* | *almost constant* | - |
| Temperature | - | - | *increases* |
| Wafer doping (p-type) | *decreases* | *increases* | *increases* |
| Wafer doping (n-type) | *increases* | *increases* | - |

2. “Organic electrolytes” (“org”). It is mixture of HF and an organic solvent including water from adding HF (49%). Large number of organic solvents can be used. The most prominent from them are acetonitrile (MeCN), dimethylformamide (DMF), and dimethylsulfoxide (DMSO). Their I(V)-characteristics do not show a PSL-peak. It is possible that PSL-peak is hidden due to the large resistance of the org electrolytes.

3. “Oxidizing electrolytes” (“ox”). This type of electrolytes is applied for anodic oxidation and contains some oxidizing reagent but always excludes F ions. Large number of electrolyte without HF addition can be classified by their “oxidizing power” according their possibility to form an oxide on Si. It can be easily measured by analyzing the V(t)-curves (Figure 7,d). They are always linear in the beginning and the value of the slope dV/dt can be the measure of “oxidizing power”.

Fourth group of electrolytes can be distinguished: “mixed electrolytes”. It contains everything not included in the groups considered above. For example, it can be mixture of “ox” electrolyte with a dash of HF, water free org electrolytes, or diluted HF with some $CrO_4$. In these cases the name of electrolyte can be changed by mixing the symbols: aqu+ox.

The main carriers of the current in the process of porous silicon formation are holes, injected from the bulk towards the interface. The current is typically maintained in the range between 0 and electropolishing threshold. There are several different mechanisms for

describing the dissolution chemistry of silicon. All of them generally accept that the holes are required for electropolishing and pores formation. Typically, the surface of silicon in HF solution is terminated by hydrogen. Consequently, the first step of surface dissolution is the replacement of a surface H with F in HF solution (Figure 8). It requires a hole to neutralized Si-F bonding. Then, there are several possibilities and two of them are represented by Figure 8 [1, 3].

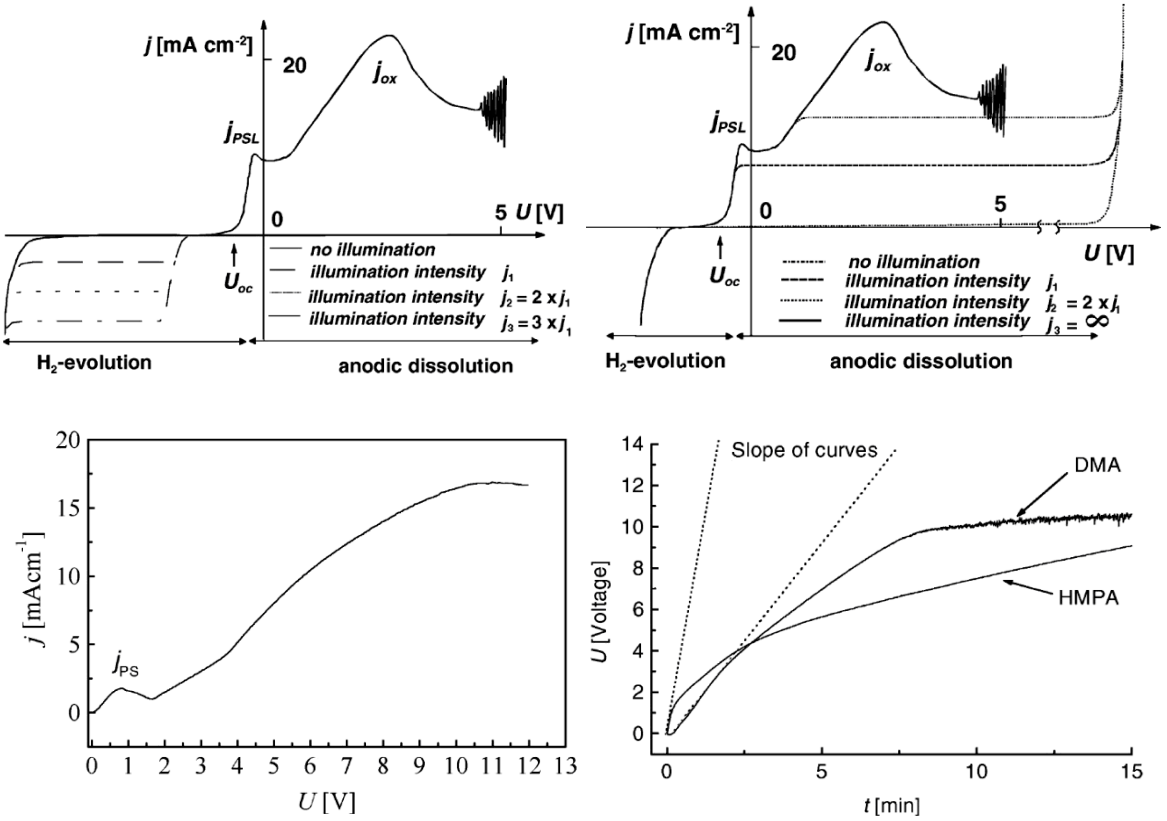


**Figure 7.** Representative *I(V)* characteristics: (a) aqu electrolyte, p-type Si; (b) aqu electrolyte, n-type Si; (c) org electrolyte (FA); (d) *U(t)* for ox electrolytes. The PSL-peak is indicated by $j_{PSL}$ [3, 4].

According to theory [3] P-Si formation occurs in three phases. Figure 9 presents three main stages of porous silicon formation (top-down): 1) initial stage, the pores develop randomly on the surface; 2) self-regulating process, pore growth change from anisatropic growth to a highly directional growth since the depletion zones around each pore overlap; 3) pore tips formation [3]. Two main techniques of P-Si formation by electrochemical anodization are considered: method of dry contact to the inactive side of silicon and fluid contact.

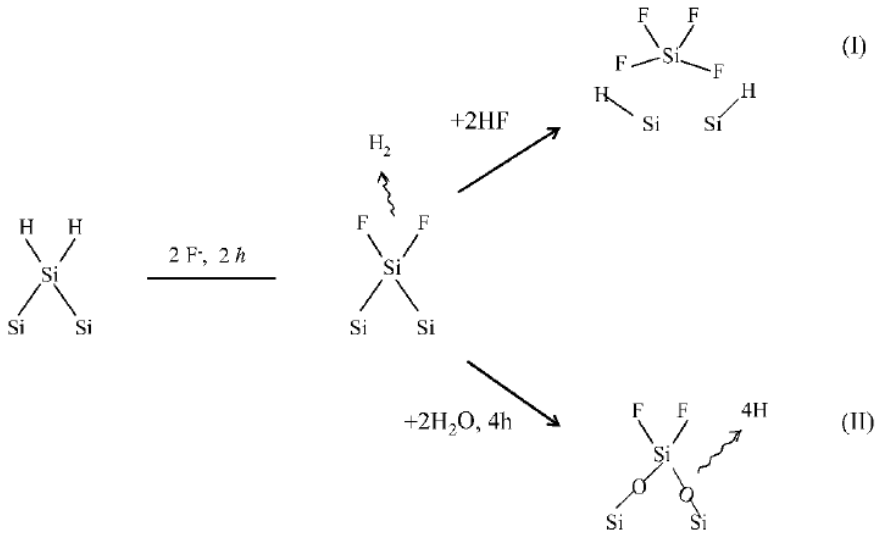


**Figure 8.** Two different reaction paths for a silicon electrode in HF solution [1, 36, 37].

The essence of the first method is the electrochemical etching of silicon in the vertical single-stage electrolytic cell. Its concept is shown in Figure 10. In order to ensure an ohmic contact at the interface anode / substrate additional doping of the surface layer is usually carried out by diffusion, or aluminum layer (thickness approximately 1 micron) is pre-applied.

The cell consists of two electrodes in electrolyte bath, i.e. anode and cathode. All structural parts of the cell are made of PTFE. Contact pad to accommodate the silicon substrate is a brass disk, mounted in fluoroplastic pedestal. A silicon wafer is placed in electrolytic cell so that the contact occurs with bottom metal electrode. The cell is filled with electrolyte. When a current flows to the anode side of the silicon wafer multistage dissolution reaction and recovery of silicon proceed. Upper electrode (cathode) is typically a platinum plate. On the surface of the silicon substrate the formation of porous silicon layer starts. Its thickness can be determined by the anodization time.

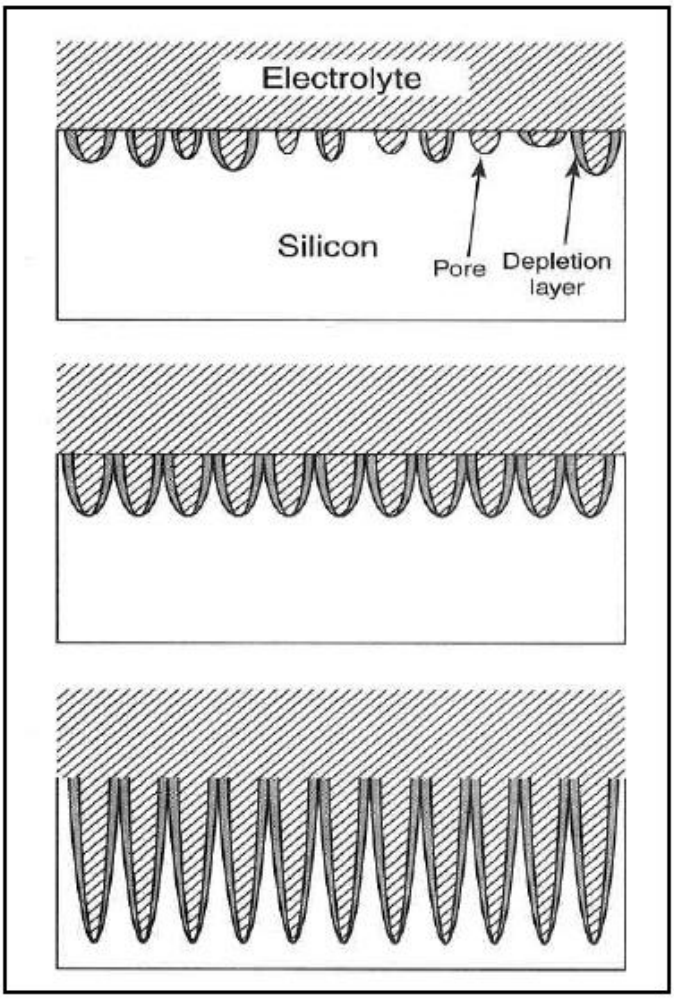


**Figure 9.** Pore formation in porous silicon [3].

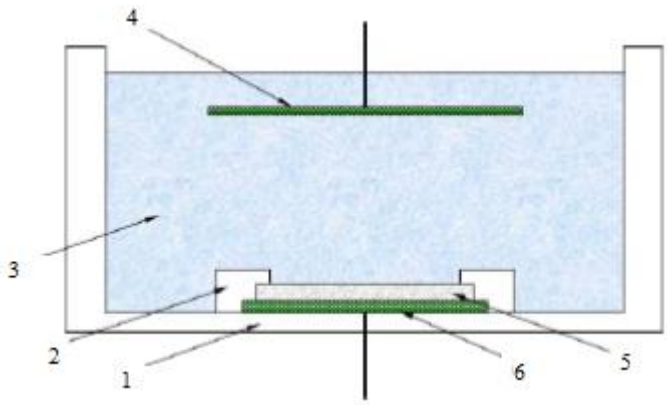


**Figure 10**. Schematic diagram of the single-stage vertical electrolytic cell 1 is PTFE bath; 2 is tight ring; 3 is electrolytic solution (aqueous solution of hydrogen fluoride); 4 is cathode-electrode (platinum-rhodium); 5 is a silicon wafer; 6 is anode - electrode (aluminum) [4].

Uniformity of forming porous layers on large-area samples can be achieved by using a cathode with area larger than the area of the sample. Another possibility is strictly coaxial disposition of the anode and the cathode.

Method of liquid contact has been developed by H. Unno and K. Imai [3, 4]. The advantage of this technique is that electrical contact with inactive side (cathode) of the silicon wafer is carried out by contacting via the electrolyte. This ensures high uniformity of characteristics of a porous layer on the wafer area and simplifies the process of preparing the plate to anodizing. Thus, there is no need to pre-form the highly doped layer or metallization layer on the inactive side.

Schematic diagram of the two-chamber electrolysis cell of Unno - Imai is represented in Figure 11 Method of fluid etching is as follows: a silicon wafer is immersed in a fluoroplastic bath and divides it into two independent volume.

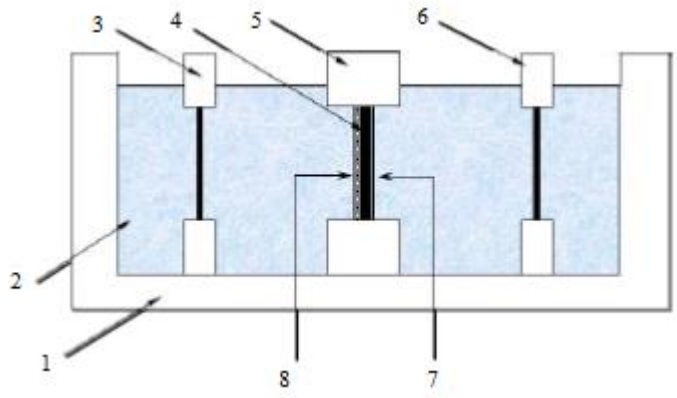


**Figure 11**. Schematic diagram of the two-chamber electrolysis cell of Unno - Imai: 1is PTFE bath; 2 is electrolyte solution (aqueous solution of HF); 3 is cathode - electrode (platinum-rhodium); 4 is a silicon wafer; 5 is the holder of a silicon wafer; 6 is anode - electrode (platinum-rhodium); 7 is cathode (inactive) side of the silicon wafer; 8 is anode (active) side of the silicon wafer [4].

The electrodes from the platinum-rhodium alloy are placed on both sides of the plate at the same distance from it. Bath is filled by electrolyte based on an aqueous solution of hydrofluoric acid. Constant voltage is applied to platinum - rhodium electrodes from the power supply operating in the constant current mode (DC). The formation of porous layer

takes place in the implementation of the pores formation conditions on active side (anode) of the plate [4].

### 2.3. P-Si modification, materials and aims

As mentioned above, porous silicon has huge range of applications. P-Si modification by other materials allows to expand the application area or to improve any characteristics required in a particular application. For example, in [38] a layer of $SnO_2$ is used in P-Si matrix to increase the selectivity of device. Also, anodes based on porous silicon modified by Pt and Ru can produce much more stable and higher photocurrent [39]. This type of electrode material maintained good electrical parameter values during several repeated tests.

Researchers in [40] examine the magnetic properties of the nanocomposites obtained by chemical vapor deposition of CoNi, Fe and FeNi alloys at different concentrations in the porous silicon. The authors note magnetic anisotropy in structure (see Figure 12). This effect is oriented along the direction of the linear cylinder and perpendicular to the plane of silicon wafer. Priced demagnetization factor of this structure is close to the ideal value which is typical for a ferromagnetic cylinder. Furthermore, the magnetic alloy deposited in channels of the silicon matrix is nanocrystalline.

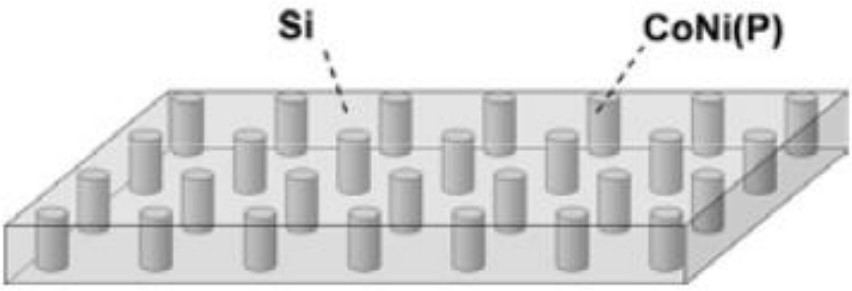


Figure 12. Model of magnetic structure with magnetic alloy cylinders in silicon matrix [40].

Porous nanocomposites based on $A_3B_5$ semiconductor [41] can be used in photonic devices. These porous nanocomposites are received by etching and anodization. Various etching conditions allow to obtain different types of porous structure. The main problem of creation of these material is the homogeneity of the porous structure, which reflects the

tendency to non-uniform nucleation. For example, the author of [42] notes that the columnar porous structure on InP formed by molecular beam epitaxy is not as uniform as compared with a similar structure in silicon formed by lithography.

The introduction of nickel particles in P-Si increases the selectivity as a gas-sensitive sensors. For example, in [43] it is reported that the nickel microgranules in a dielectric matrix can catalyze the decomposition of methane at elevated temperatures. Thus, the researchers have found these significant increases sensitivity of nanocomposites porous silicon - nickel to adsorption of methane molecules at elevated temperatures, i.e. solid methane gas sensor can be based on this structure. Oxides of tin, iron and nickel formed by sol-gel method on porous silicon also allow to increase the sensitivity to acetone vapour [44]. Nanocomposites of nickel ferrite can also extend the sensitivity of detectors to environmental changing [45].

Another target described in [46] is the increase of photoluminescence intensity. This parameter in system of P-Si – Ni particles is about 11 times stronger than that of P-Si. One more application of Ni on P-Si can be high performance anode for Li-ion batteries [47 - 49]. For instance, work [49] describes the accommodation of large volume vibration of Si during cycling and facilitation fast transport of electrons and lithium ions by this electrode.

## 2.4. Surface modification techniques

Previously, materials and goals for the porous silicon modification were reviewed. Few methods of surface modification should be mentioned. Each method has its advantages and disadvantages, so in this section both methods of porous silicon modifying are considered.

### 2.4.1. Electro-chemical deposition

Electrochemical deposition is inexpensive and fast technique. It has a number of applications in microelectronics, semiconductor industry and fabrication of materials for different purposes [50]. The essence of the deposition process is in recovering the metal ions dissolved in the conductive solution on the electrode surface.

Typically, the cathode coating is conductive. Therefore, the deposition process can continue indefinitely until the corresponding metal ions are in solution and current flows

through an electrochemical circuit. The structure and properties of the cathode coatings are determined by main parameters of the cathodic process: current density ($A/m^2$), voltage (V), temperature ($^oC$), duration (s), conditions of mixing (rpm) and composition of the solution. The quality of deposited coatings have a significant impact of the cathode surface preparation and electrical properties of the electrolyte. Furthermore, there is a high probability of parallel reduction reaction of hydrogen and its incorporation into the films during the cathodic deposition. This leads to a decrease in mechanical resistance of coatings, formation of pores and other undesirable consequences.

The determination of thickness *h* of the deposited coating is based on Faraday's law with formula $h = \frac{V_m}{zF} jt$, where $V_m$ is a volume of one mole of metal, *z* is amount of ions and *F* is Faraday's constant. The formula implies that the deposition rate is proportional to the current density. In other words, uniform current supply to the entire deposition surface is necessary to obtain a uniform coating thickness.

Uniform current supply is connected with uniformity of distribution pattern of the electric field in the cell. This is a consequence of Ohm's law $j = \sigma E$, where *E* is the electric field strength and σ is electrical conductivity of the electrolyte.

The current density will be different if two regions of the cathode surface are at different distances from the anode. Various methods are used to increase the uniformity of the deposition rate. They involve finding of the optimal conductivity and the concentration of the electrolyte and the form of electrodes and cells. Often the design of electrochemical baths includes special screens and perforated septum.

Surface roughness significantly affects on the uniformity of the current. Typically, the current density on the microtips is higher, while in the microcavity current is lower. Consequently, the roughness increases during deposition. The leveling additives are added in electrolytes to prevent this phenomenon. These additives inhibit the process of separation of the metal. It is more effective in case of greater density current flowing through the active surface part.

Levelling additives provide deposition special coating, so they are often called additives of luster. Acetylene alcohols, aromatic aldehydes, azo dyes, ketones and a number of sulfur-containing organic compounds have strong luster effect [51].

### 2.4.2. Sol-gel method

The phrase "sol-gel" began to be used since the late 1980s referring materials formed as a result of gelation (sol-gel transition) and the processes that underlie this phenomenon [52, 53]. Sometimes, sols are divided into colloidal sols and polymer in contemporary literature. Thus, the dispersed solid phase is usually formed by particles in colloidal sols, while polymer sols are formed based on branched macromolecules. Mechanisms of gelling in colloidal and polymeric sols are different.

Gel from the polymer sol is formed during the polymerization of the monomers and the polymers. Gradually branched oligomers form a giant cluster. When the cluster reaches macroscopic dimensions and extends to the entire volume of the sol, it is considered there was a transition sol-gel. On the one hand, this gel is composed from a continuous structural grid (solid skeleton or core). On the other hand, there is a continuous liquid phase.It is the different mechanism of gel formation from a colloidal sol. The particles of the dispersed phase (micelles) interact with each other under the influence of dispersive attractive forces and form an inorganic polymer backbone [52].

According to modern concepts of Sol-gel method, the gel formation begins with the formation of the fractal structure. The growth of fractal aggregates continues until they begin to encounter and engage with each other. It is described by the percolation theory [52, 54, 55].

All major processes that occur during the sol-gel transition and products obtained by sol-gel synthesis are schematically shown in Figure 13. Thus, the term "sol-gel process" means the technology of obtaining inorganic and hybrid organic-inorganic material (catalysts, adsorbents, ceramics and other composites) based on the transformation in homogeneous solutions and then in the sol gel [52].

Precursors are required to form a sol. Typically, they are compounds capable to hydrolysis: metal alkoxides $Me(OR)_n$, where M is metal, OR is alkoxyl groups (e.g.$CH_3O^-$, $C_2H_3CH_2O^-$ ), salts and acids. Alkoxides, where silicon takes place of the metal, are called alkoxy $Si(OR)_4$. They are often used for the purposes of microelectronics. The basic structure-forming processes in the sol-gel systems based on alkoxy are as follows:

$$(RO)_3{=}Si - OR + HOH \Rightarrow (RO)_3 = Si - OH + ROH$$

$$\text{or} \quad = Si - OH + RO - Si = \Rightarrow = Si - O - Si = + ROH$$

or = Si – OH + HO – Si = => =Si – O – Si = + HOH.

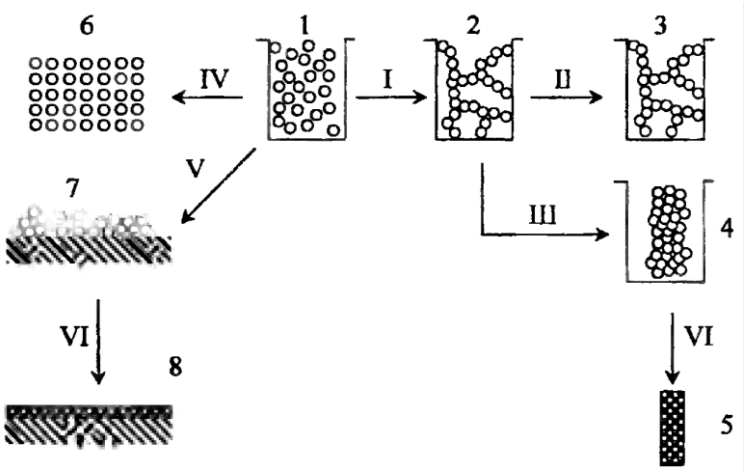


**Figure 13.** Schematic diagram of the preparation of various materials, coatings and powders by sol-gel technology. The figure introduces the following indications: I is maturing and gelling the sol: sol (1) → gel (2); II is drying under supercritical conditions or the gel ablution in solvents: gel (2) → airgel (3); III is conventional drying conditions: gel (2) → xerogel (4); IV is nanoparticles deposition: sol (1) → powder (6); V is the application of the sol on the substrate: the sol (1) → xerogel film (7); VI - burning: xerogel (4) or xerogel film (7) → monolithic glass and ceramics (5) or the film and coating (8) [52].

The rate and the completeness of their occurrence depend on the chemical and technological factors, namely the nature and quantity of alkoxy compound, water, acidity (pH) of the environment, the nature and amount of organic solvent, homogenization techniques sol-gel systems, the temperature and duration of the synthesis.

Structuring processes occur in the sol with the deepening of the processes of hydrolysis and condensation. They are accompanied by an increase in viscosity and completed by the transition to a gel.

One of the most common precursors most frequently used in the sol-gel technology is a typical representative of alkoxy ethyl ester of orthosilicic acid, or tetraethoxysilane (TEOS). The most interesting feature of the sol-gel-systems based TEOS is that they can be doped with metal alkoxides or inorganic compounds (acids, metal salts). This feature is most interesting for applications in micro- and nanoelectronics. These dopants form nanocomposites on porous silicon and can give the necessary properties (catalytic, electrical etc.) [52].

## 3. Methodical part, concepts of NanoScience

Richard Phillips Feynman, the famous American physicist, one of the founders of quantum electrodynamics, Nobel Prize 1965, was the first to speak about the concept of the molecular and nanotechnology. He gave a lecture "There's Plenty of Room at the Bottom" at the California Institute of Technology at the Christmas dinner of the American Physical Society on the eve of 1960. In this chapter "below" means "world of very small size". Feynman discussed the possibilities of scientific and technological areas, which today is called "nanotechnology". Renowned physicist argued that in the distant future (2000 year) people will be surprised that had not paid enough attention to nanoscale science. He drew attention to the fact that each person has "tamed" nanoworld. It means we all are composed of minute details, cells. He also claimed that the microcomputer incorporated in each person, easily cope with the tasks, prohibitive for most modern for its time computing systems. Feynman thought the reason for this is that inside our body microcomputer (in our skull) is a number of logic elements, which at times exceeds the number of elements in the high-end computer system. This led him to the idea of creating a submicroscopic elements [56].

He also considered few possible problems and benefits of moving to the nano-size science. He believed, for example, that it is possible to create a system of robots that will autonomously create their reduced copies (Figure 14). However, this will lead to unusual physical phenomena with decreasing size. Insignificant weight of items, nanorobot will lead to the fact that they will adhere to each other by intermolecular forces. For instance, the nut will not separate from the bolt after untwisting. However, the known laws of physics do not forbid to create objects "atom by atom." Manipulation of atoms, in principle, is very real, and does not violate any laws of nature. The practical difficulties of its realization is caused only by the fact that we ourselves are too large and bulky objects. Therefore, it is difficult for us to carry out such manipulations.

To stimulate the creation of microobjects, Feynman had promised to pay $ 1,000 to the person who built an electric motor with size of 1/64 inch (1 inch ≈ 2.5 cm). Soon this mikromotor was created (Figure 15). Since 1993 Feynman Prize is awarded annually for outstanding achievements in the field of nanotechnology.

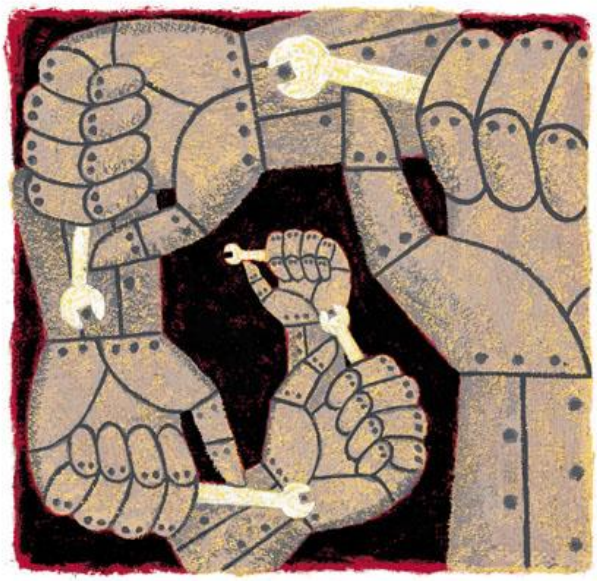

**Figure 14.** Concept of Feynman how robots will be autonomously create their own smaller-bodied counterparts [56].

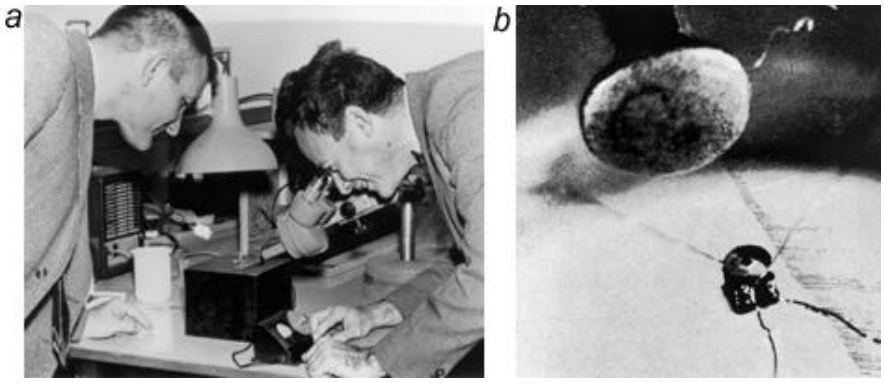


**Figure 15.** a) Feynman examines a micromotor 380 microns in size using a microscope, b) micromotor 380 microns in size and the head of a pin [56].

### 3.1. Scanning probe microscopy (SPM), its history and basics

Yang profilometer is considered as the first scanning probe microscope [57]. It detects a field emission current between a scanning metallic tip and the sample surface. Young experimental approach was developed brilliantly in the works of G. Binning and H. Rohrer. In 1982 they developed the scaning probe microscope to image the surface topography [58]. It led to the emergence of a scanning tunneling microscope with atomic

spatial resolution. They were awarded the Nobel Prize for Physics in 1986. They were successful to observe single monolayer, only one row of atoms with height of 1 atom.

Gerd Binning and Christoph Gerber started to implement Binning's idea after relocating to California in 1985. His idea was to create atomic force microscope. In 1986 Binning, Quate and Gerber reported experimental data of a sapphire surface with lateral features spaced 3 nm apart-far from atomic resolution. In this paper the authors also presented a plethora of visionary ideas on how to improve the AFM's resolution, including oscillating-cantilever [59].

The main components of a scanning probe microscope (Figure 16) are: probe, scanner and detector. To carry out the work, analog electronics are also required. It will convert the signal from the detector and transmit it to a computer graphics system, with which one can either watch the process or control and manage it.

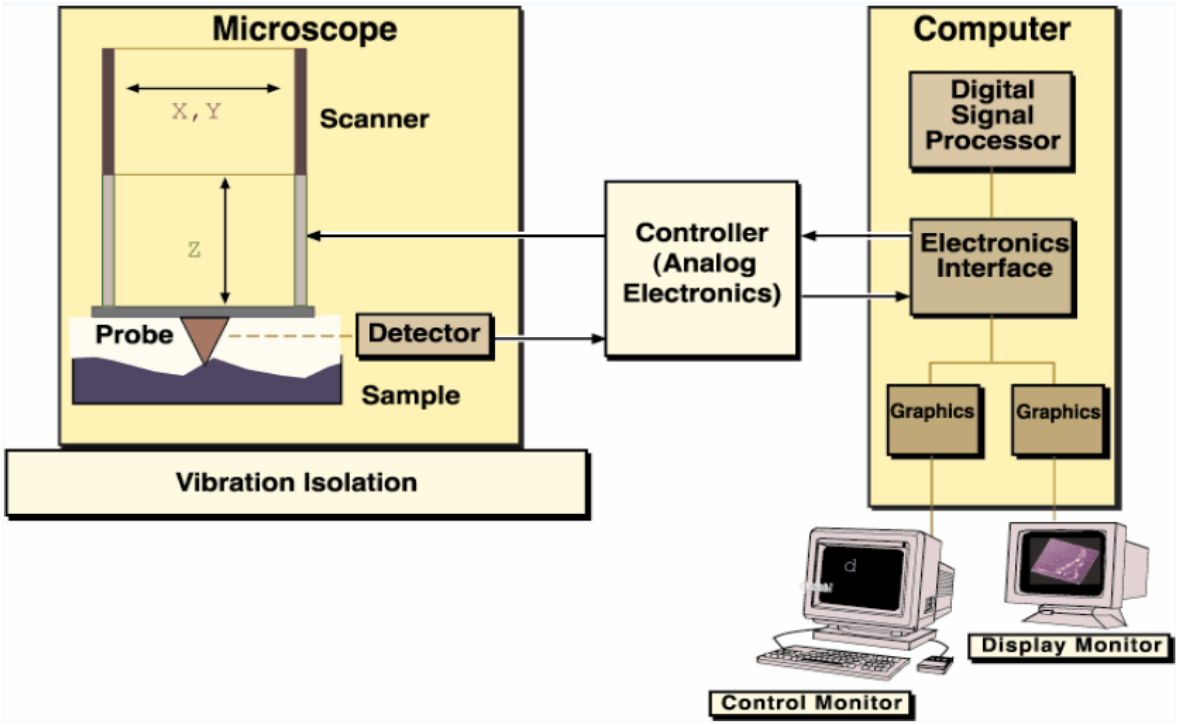


**Figure 16.** Main components of a scanning probe microscope.

A probe tip is usually made of W or Pt–Ir alloy. It is attached to a scanner, which consists of three mutually perpendicular piezoelectric transducers: x, y and z piezo. Scanner is made from piezoelectric ceramics. Thus it expands or contracts upon applying a

voltage. A tunneling current is generated by applying a bias voltage between the tip and the sample.

Typically, the tip is virtually grounded. The bias voltage $V$ is the sample voltage. When $V>0$, the electrons are tunneling from the occupied states of the tip into the empty states of the sample. In opposite case, the electrons are tunneling backwards. The current amplifier converts tunneling current to a voltage and compares it with a reference value. Negative feedback is provided in the device: if the absolute value of the tunneling current is larger than the reference value, then the tip is withdrawn from the sample surface, and vice versa. It is a method to establish an equilibrium $z$ position. When the tip scans over the $xy$ plane, a two-dimensional array of equilibrium $z$ positions is obtained, displayed, and stored in the computer memory. It represents a contour plot of the equal tunneling-current surface. The surface topography is displayed on a computer screen [60].

### 3.2. Atomic force microscopy (AFM)

The hands touching the surface is the main concept of AFM working (Figure 17). Atomic force microscope uses the force of interaction between atoms, feels the surface and creates an image of the surface. It is considered that the interaction of surface - probe is regulating by short-range chemical-bonding forces and long-range van der Waals, electrostatic, and magnetic-dipole forces. The interaction between the tip and the surface atoms is described by the Lennard-Jones potential (see Figure 18). On this curve, there are zones of contact and non-contact mode [59].

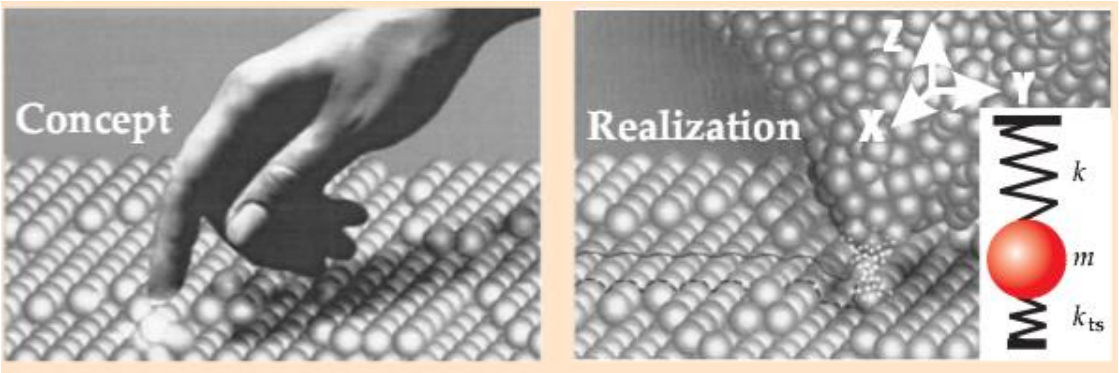


**Figure 17.** Concept and realization of AFM work [59].

In contact mode the probe pushes the surface. The strength of the applied pressure is set in the system parameter "SetPoint" in such way that tip does not create destructive

effect on the surface. AFM image is formed by pixels (Figure 19). First, the probe goes straightway, then returns, “rises up” and passes through another line.

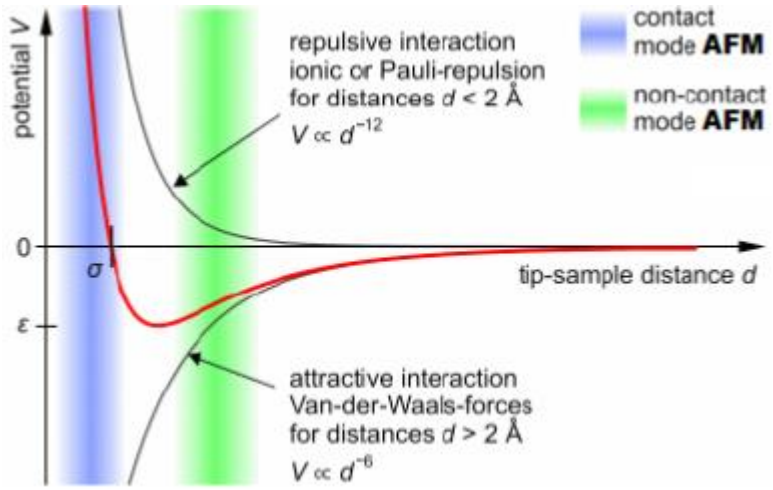


**Figure 18.** Lennard-Jones potential curve [61].

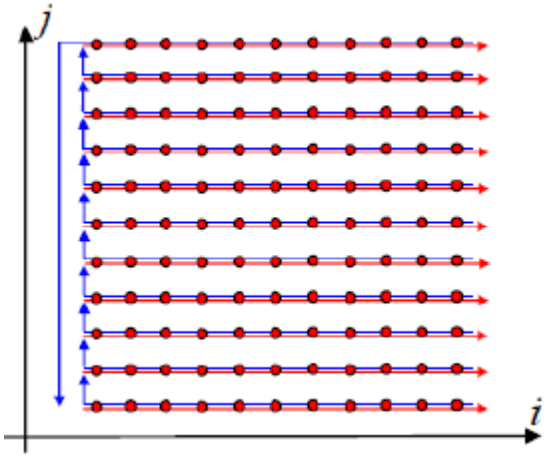


**Figure 19.** Scheme of scanning process: red is straightway, blue is forward (*j* is number of pixel line, *i* is number of position) [62].

Two modes of AFM exist: constant force and constant distance (Figure 20). It should be noted that Contact Mode is not used with soft materials or living objects because of the significant forces applied to the sample surface (nN).

Semicontact mode (Figure 21) can be also used. Initially the probe is vibrating with cantilever's resonant frequency without touching the surface. When tip is approaching to the surface, repulsive force is increasing and oscillation amplitude is decreasing. Thus sample is moving by feedback from the tip until amplitude becomes initial. In this mode

probe impact on the surface is more gentle. Consequently, it is applicable even for living cells.

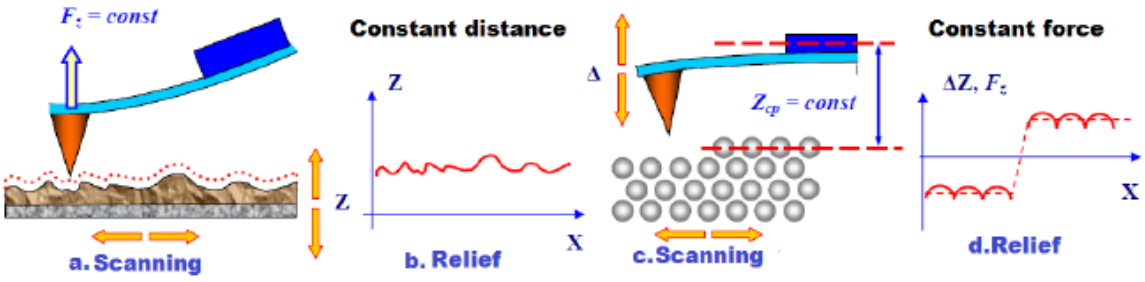


**Figure 20.** AFM constant distance (a) and constant force (c) modes with topography (b, d) [62].

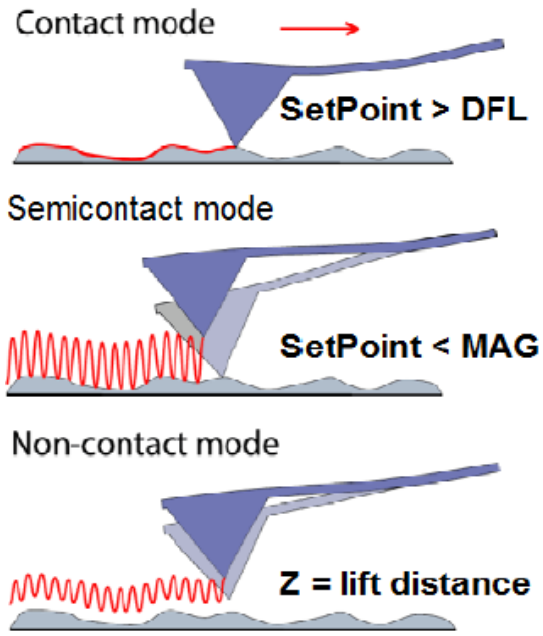


**Figure 21.** Principles of AFM modes [62].

Tip is oscillating with its own resonant frequency and is not touching the surface at all in Non contact mode (See Figure 21). The half-amplitude of oscillations is less than distance between surface and cantilever's middle line (lift height). This mode is used as a part of “two-pass” technique. In first pass the Semicontact topography is measured. In second pass the strong long-range forces can be measured [62].

Figure 22 represents basic components of AFM: probe (consisting of cantilever and tip), sample on top of scanner and photodetector.

**The probe** usually consists of a pyramidail form tip fixed on the flexible cantilever (Figure 23). Probes are made of Polysilicon or $Si_3N_4$. The probe is characterized by following parameters: 1) tip radius; 2) cantilever spring coefficient and 3) cantilever resonant frequency.

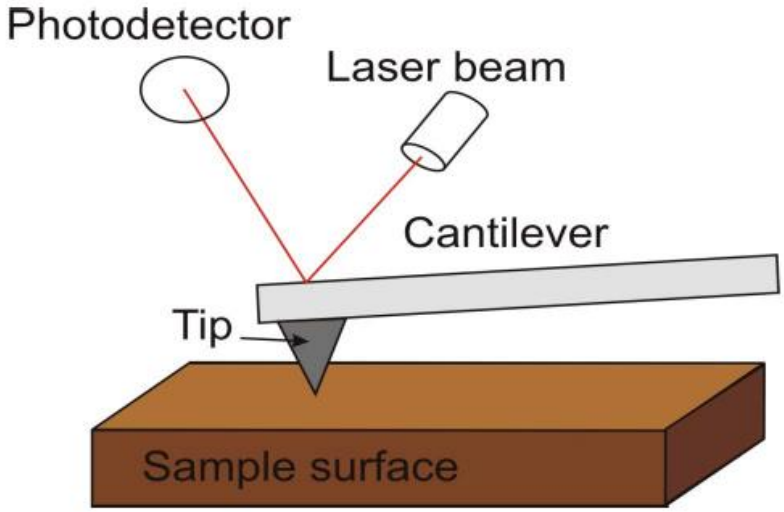


**Figure 22.** Basic components of AFM.

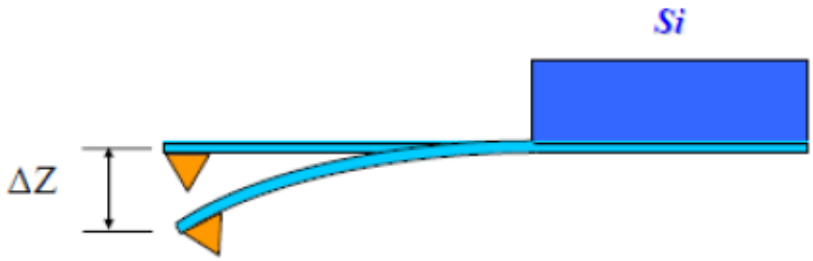


**Figure 23.** The cantilever scheme [62].

**The Scanner** is a device that provides sample movement relatively to the AFM probe. This device consists of a radially polarized piezo ceramic tube and is coated with metal electrodes on four sides. Electrodes are required to realize the piezoelectric effect for precise movements of scanner. There exist two types of the scanner mounting: ”by sample” and ”by probe tip”. In first type the sample holder is attached to piezo-scanner. Pattern is measured more accurately due to the optical detection systeme is not moving. In second case piezo-scanner is attached to the probe. Scanner provides the probe movements in three dimensions ($x$, $y$, $z$). The range of scan areas can be from few nanometers to several tens of microns.

Piezo-scanner has limitations: nonlinearity, creep and hysteresis properties (Figure 24). The first effect is the deviation from linear dependence of the length change. The second phenomenon is connected with delay in response to the controlling voltage. Third, hysteresis properties of piezo ceramic tube in length changings cause inaccuracy. This is the reason to carry measurement in one direction.

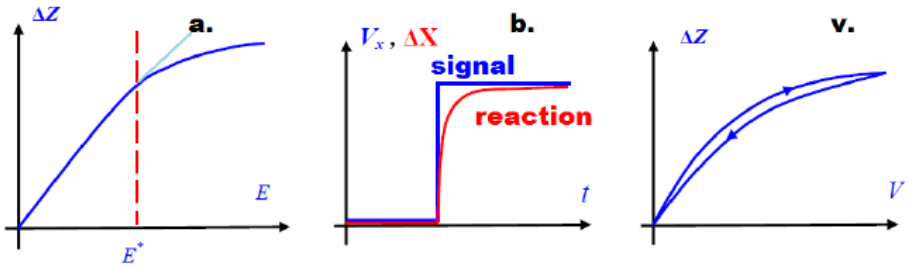


**Figure 24.** Piezo ceramics deficiencies: nonlinearity (a), creep (b), hysteresis (c) [62].

**Photo detector** is the device to measure the deflection of the probe. The optical detection system measures the cantilever bending and consists of laser source and 4-sectional photodiode. Laser light is pointing onto cantilever and is reflecting to photodiode.

**The feedback system (FB)** provides a constant influence on the probe [62].

### 3.2.1. PeakForce® QNM mode

PeakForce QNM (Quantitative Nanomechanical Property Mapping) provides investigations without complexity of operation and interpretation. Moreover, it does not require special probes. Image formation (scanning speeds and number of pixels) is similar to TappingMode. Force curve data is analyzed simultaneously with a map of multiple mechanical properties which has the same resolution as the height image. Direct control of normal forces and thus the deformation of the sample is provided during the measurement. Additionally it preserves the sample and tip. There is a feature which automatically can adjust scanning parameters in real-time to optimize the image and protect the probe and sample.

The unambiguous and quantitative modulus and adhesion data provided by PeakForce QNM can help researchers study the material characteristics in more details. Moreover, it is possible to study the variation and position of mechanical properties across a surface with inaccessible at previously resolution. This mode is non-destructive to both probe and sample surface due to direct control of peak normal forces and minimizing of

the lateral force on the probe. Additionally, mechanical property maps are quantitative, when tips and measurement are pre-calibrated and have low noise [63].

### 3.2.2. Kelvin Probe Force Microscopy (KPFM)

The Kelvin method of investigation was the first postulated by Lord Kelvin in 1861. It is a non-contact and non-destructive measurement method to measure difference in surface potentials on different locations [64]. Nonenmancher presented KPFM for the first time in 1991 [65].

KPFM is considered as a "two-pass" microscopic study of surface potential [66, 67]. In first pass the topography is measured in Semicontact mode. Probe is uplifted before the second pass. The magnitude of electrostatic interaction between sample and oscillating probe is studied.

KPFM measures a contact potential difference (CPD) between the sample surface and the tip. $V_{CPD} = \frac{\varphi_{tip} - \varphi_{sample}}{-e}$, where $\varphi_{tip}$ and $\varphi_{sample}$ are the work functions of the sample and tip, $e$ is the electric charge. Fermi levels of both materials are aligned with direct contact and applied electrical potential. Thus potential of the sample will shift to the level of tip. Thereby, this method permits to calculate the work function of surface area, if the work function of AFM tip is known [68].

### 3.2.3. Magnetic Force Microscopy (MFM)

In this AFM mode tips with special magnetic coating are used. The cantilever is above the sample. The magnetic force causes cantilever bending and vertical movement of tip. According to Hooke's law, this movement is determined by the spring coefficient of the cantilever. The bending is detected by optical sensors as it is mentioned above.

When a rough surface is scanned, there is a contribution from the topography. It should be separated from the signal of magnetic forces. For this purposes tip scans surface twice. In the first pass, topography of sample surface is obtained. Magnetic properties have no effect on the observed topography. In the second pass, probe is moved above the sample surface. Thus the tip is affected by long-range forces, not by "contact" forces. The tip deviation depends on the magnetic properties of the sample [69].

## 4. Experimental part

In this Chapter the methodology of our study is presented with experimental sequence. Information about the samples is important. For example, the technological conditions of creation, expected properties (roughness, conductivity), advanced visual information (reflection, contaminants, fractures) seems significant for the researcher. Frequently required information is missing. This may cause some difficulties for the operator of the scanning probe microscopy and entail mistakes in experiment. For instance, if the sample contains any artifacts or contaminants, the results of the study may be inaccurate. In this case, it will not provide reliable information about the surface and the properties of the sample. While the characteristics of the defect will be investigated. This is associated with high locality of SPM data.

SPM operator should consider available information on the test samples and the possibilities of the microscope (its modes) in the formulating a task. Definite impact on the sample gives reaction in real-time and understanding this reaction is in personal experiment sense. Meanwhile, critical mistakes can be prevented by an approximate first probe experiment. Below is the sequence of measurements, which can be assumed as universal for this work.

### 4.1. Sample preparation

Silicon of n-type conductivity doped with boron was used for preparation of porous silicon. Samples were obtained by dry contact in the electrolyte solution (hydro alcoholic solution of hydrofluoric acid HF). Two series of porous silicon at a current density $j_a$ = 2 mA / cm$^2$ and at $j_a$ = 20 mA / cm$^2$ were obtained. More detailed process conditions are shown in Table 4. In total, 12 samples were prepared. Samples 1 and 7 were not Ni modified, they were kept to detect differences in the modification.

**Table 4.** Technological conditions of porous silicon preparation.

| **Sample number** | **Technological conditions** | | |
|---|---|---|---|
| | **Silicon type** | **Current density, mA/cm$^2$** | **Anodization time, min** |
| 1–6 | n-type of conductivity, resistivity is 12 Om·cm | 2 | 15 |
| 7–12 | | 20 | |

Two methods of porous silicon modification were chosen: electrochemical deposition of nickel (Samples 4, 5, 6, 10, 11, 12) and Ni deposition from $NiCl_2$ solution (Samples 2, 3, 8, 9) (see Table 5). An alcohol solution of $NiCl_2 \cdot 6H_2O$ was selected as an electrolyte for deposition. Electrochemical deposition was performed with bias of $U$ = 2V of different duration. Additional three samples on silicon were created to compare its surface characteristics and properties with P-Si modificated by Ni (Si-Ni 1, Si-Ni 2 and Si-Ni 3).

**Table 5.** Technological conditions of modification.

| **Sample number** | **Modification methods** | | |
|---|---|---|---|
| | ***Extract*** | ***Electrochemical deposition*** | |
| | ***Time, days*** | ***Potential, V*** | ***Time, min*** |
| 2, 8 | 1 | – | – |
| 3, 9 | 15 | – | – |
| 4, 10, Si-Ni 1 | – | 2 | 20 |
| 5, 11, Si-Ni 2 | – | | 40 |
| 6, 12, Si-Ni 3 | – | | 60 |

### 4.2. Measurement sequence

In this chapter is presented basic operational principles of Bruker Multimode 8 atomic-force microscope. Measurements and data operating are conducted with the help of "Nanoscope" software package.

Preliminary, all the equipment should be turn ON and warm up for few minutes.

1) Selection of probe. Every AFM measurement have requirements to the probe, so it is very important to select correct probe according to investigation mode and material type. For example, ScanAsyst-Air was used to measure sample topography. Its shape is triangular, tip height is 2.5 – 8 μm, tip radius ranges between 2 – 12 nm, its length is 115 μm, width ranges between 20 – 30 μm, resonant frequency is 70 kHz and spring constant is 0.4 N/m. ScanAsyst-Air allows to image sample topography with high resolution. MFMV enables MFM imaging and have rectangular shape. It is covered by hard Cobalt-Chromium tip coating for high-sensitivity and magnetic contrast. Its shape is rectangular, tip height

ranges between 10 – 15 μm, tip radius is 40 nm, its length is 225 μm, its width is 28 μm, resonant frequency is 75 kHz and spring constant is 2.8 N/m. KPFM mode needs PF-QNE-AL probe. It provides high resolution electrical measurements by matching the softness of a nitride cantilever with the sharpness of an uncoated silicon probe. Its shape is triangular, tip height ranges between 2.5 – 8 μm, tip radius is 12 nm, its length is 42 μm, width is 40 μm, resonant frequency is 300 kHz and spring constant is 0.8 N/m. NCHV was used for AFM investigation of sample cross-section. Its shape is rectangular, tip height ranges between 10 – 15 μm, tip radius is 10 nm, its length is 125 μm, width is 40 μm, resonant frequency is 320 kHz and spring constant is 42 N/m. It can conduct imaging in TappingMode™ and non-contact mode in air [70].

2) The probe and sample installation. Not all processes in the atomic force microscope are operated by device or computer. Some actions are performed manually. One example, is to install the probe and the sample. Since this procedure is delicate and is done manually, it requires a definite algorithm.

Probes are stored in special boxes with an adhesive coating in the bottom. Shape of probe is rectangular. At one end the naked eye (though with difficulty) can see a small dot and this point is the cantilever. The dimensions can be designated downwardly: Probe (5 mm) - cantilever (40 μm) - tip (5-10 μm) - tip's apex (15 nm). Cantilever can be seen only with the help of optical microscope. Tip's apex touching the surface can be viewed in the electron microscope.

The probe should be installed with the help of tweezers. One pulls out the probe from its box by the short side and installs the probe in the probe holder. A special mechanism presses the probe, so it does not fall and does not move. This holder is installed in the device of the microscope over the piezotube, with which it has a feedback.

The sample of investigation is placed on a plate and fixed. It is put on the piezo-tube (it is necessary to avoid damage) and is electrically grounded. The measuring Head with probe holder is lowered over the sample in distance of 3 mm (approximately) with the help of Head's screws. Otherwise the tip can touch the surface and can be damaged. In this case the measurements will not be of high quality.

3) Setting the probe. A laser should be configured to the cantilever before starting the measurement. For this purpose an optical microscope is used. Focus is tuned to the probe. With the help of a laser sensor's screws the laser spot is introduced to the optical microscope and configured from entering the probe. Next step is to select the maximum (or near maximum) value of the intensity of the laser with the help of data on the screen of atomic force microscope. Photodetector's screws help in looking for its position when the intensity value is zero (or close to the zero value). The image of laser spot in an optical microscope should not significantly displace from the probe.

4) (Surface approach) Starting of measurements. In connecting to the device via the Bruker software a choice of operating modes is offered. After selecting the operating mode for the study the operator starts the SPM probe approaching to the surface and installs the necessary parameters for the investigation. The procedure for the probe approaching to the surface is quite delicate and complex: in the process the surface may damage the probe. Firstly, the operator sets an optical microscope on the surface of the sample. Secondly, with the help of measuring head's screws he begins to approach it to the sample surface. It should be possible to safely bring the probe to the surface. Further approximation is done electrically by program of the atomic force microscope.

Measurements setting includes selecting the size of area to be scanned, the scanning speed (also depends on the size of the scan area), pressure force of the probe to the surface, the output data and much more. For example, in tapping mode it is also necessary to determine the resonant frequency of the cantilever and select the operating resonant frequency.

There are a number of artifacts, which should be avoided during investigation. They can be caused by:

1. Incorrect probe selection. Each probe has its stiffness. This parameter is always specified by the manufacturer on the packaging. Some probes have a stiffness of about 0.1 N/m, while others have much larger stiffness, of about 100 N/m. For instance, using a probe with a high stiffness in soft materials investigation can damage the surface in the contact mode.

2. Wrong selection of pressure force. In this case, the probe may become unavailable. Then there will be a so-called probe convolution, i.e. repetition of one picture on the entire image. For example, in the figure 25 the repetition number of the triangular structures can be seen, but they are not actually existing on the surface.

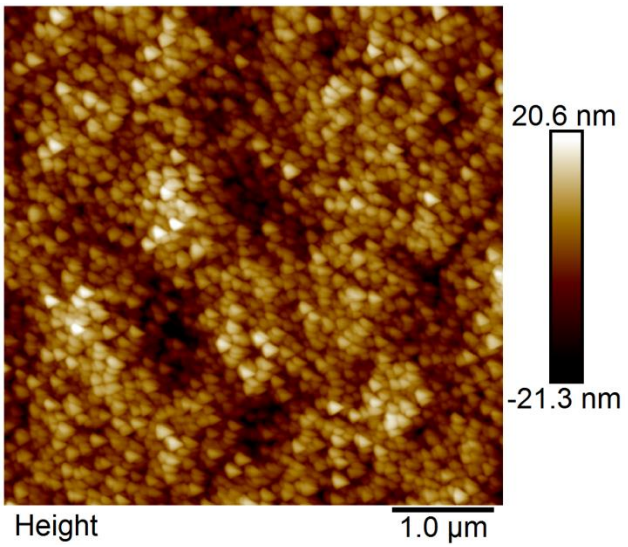


**Figure 25.** Example of probe convolution on the sample #8.

The above-mentioned artifacts can be reduced by conditions of measurement. The system parameters, procedures and settings shown above seem to be valuable for practice. Meanwhile, some operations can be called in different way in other systems and several procedures can be done automatically in more advanced devices. Nonetheless, the experience and skills are required for proper operation of the SPM. The results of investigations of Ni particles deposited on porous Si presented below are obtained with the help of the methodology described above.

## 5. Results

In this section, the results of topography, MFM, KPFM and cross-sectional data will be discussed and compared with other authors.

### 5.1. Topography

The topography of the samples was obtained by using PeakForce Mode. To compare methods and quality of the obtained images topography of the sample #8 was made by tapping mode (Figure 26). The data are comparable, but the PeakForce method is more accurate and allows to protect the probe. The resulting images show comparable topographies with images from other authors [71, 72] (Figures 27, 28), considering the z-height data scale bars.

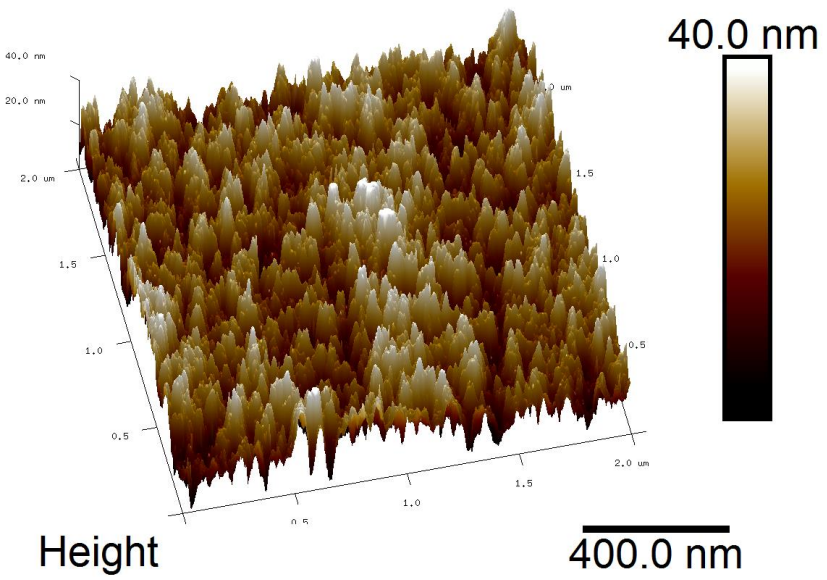


**Figure 26.** The 3D-recovery of surface topography for sample #8 (tapping mode). 2μm, heightscale 40 nm.

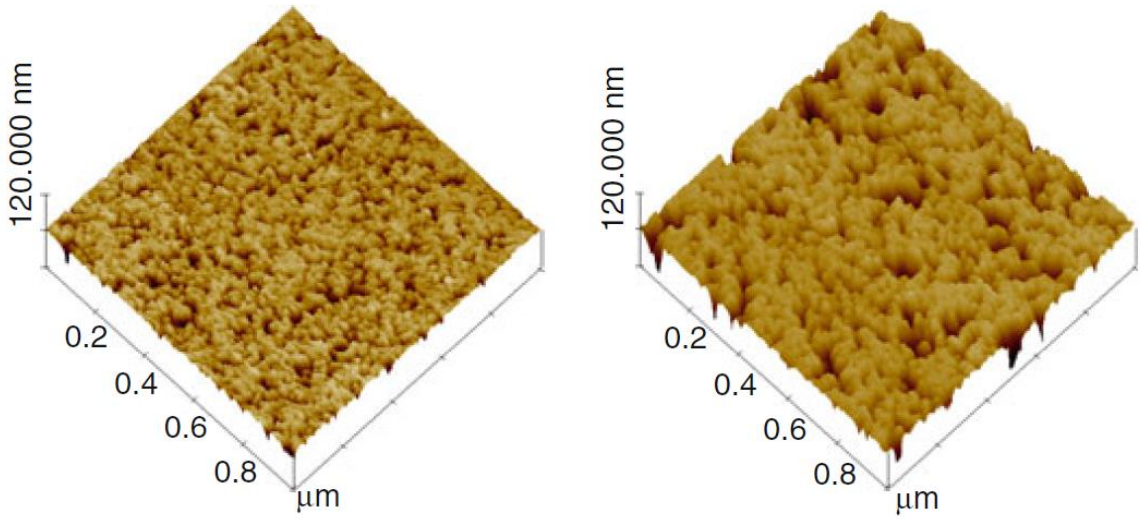


**Figure 27.** Surface of two diferrent porous silicon determined by AFM [71]. 1 µm, height scale 120 nm.

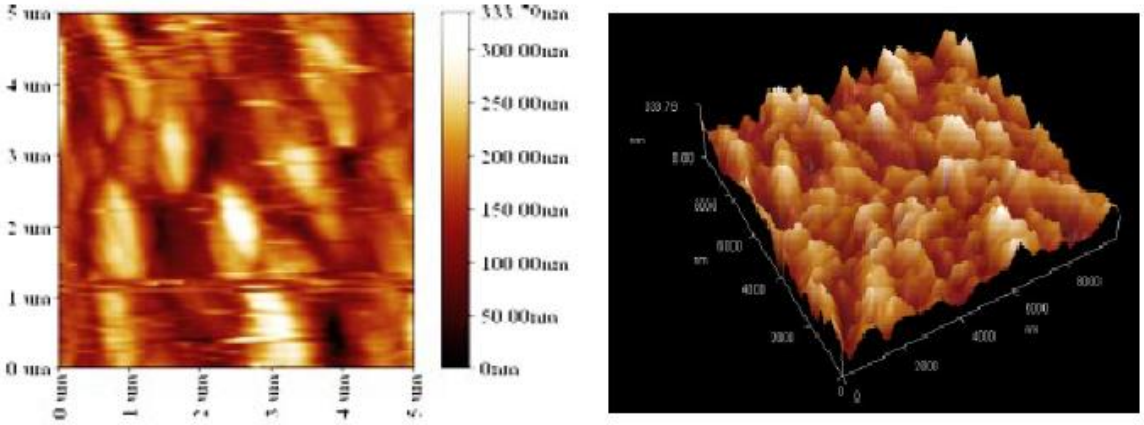

**Figure 28.** 2D and 3D AFM images of porous silicon surface [72].

Topography data was processed by third degree curves for smooth images as initial AFM files always have a curvature. We know, meanwhile, that surfaces are 1D level.

According to the AFM data one can suggest the impact of treatment on the surface. For example, images of samples 1 and 7 (Figure 29) show that different roughness can be obtained under other conditions of the silicon surface etching. Figure 30 presents silicon monolayer with the height of 215 pm. Approximately 17 layers are observed on it, totally 3.5 nm in the height. While comparing figures 29 and 30 it can be noticed that etching has influence on surface and it is not artefacts. The impact of the treatment by nickel can also be noticed. After exposition from a solution the surface becomes smoother (Figure 31). With a more long-term electrochemical deposition shown an increase of roughness (Figure

32). Perhaps, size of particles increases. It can be seen from the Table 6 which shows roughness of all samples in two different areas. The parameter can indicate the presence of pores and particles on the surface. Disadvantages of the investigation method include the fact that when measuring small pore size (in this case micropores), the probe may be greater than pores. In this case fully pores can not be investigated. The probe will touch only the top part of pores.

Moreover, particles (pores) are visible in the investigation of samples by the optical microscope (Figures 33, 34). Their density and size correspond to the treatment condition: in the beginning, the surface becomes more smooth (after particles deposition) then more developed (because of their growth).

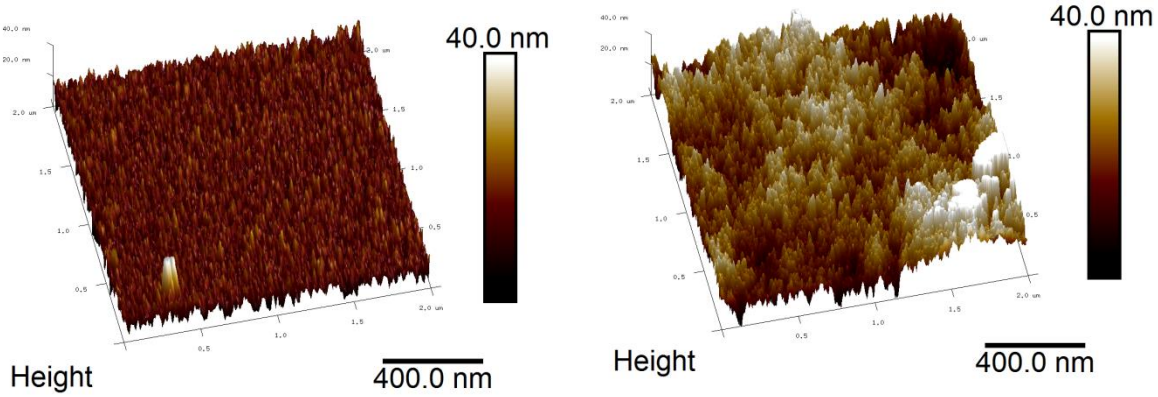


a b

**Figure 29.** The 3D-recovery of surface topography for samples 1 (a) and 7 (b).

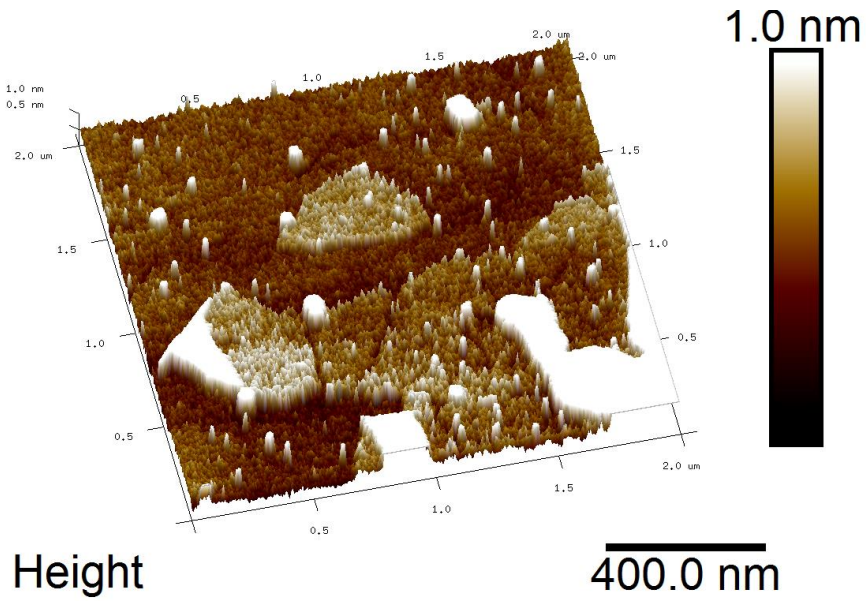


**Figure 30.** The 3D-recovery of one monolayer of silicon, clearly visible on the center.

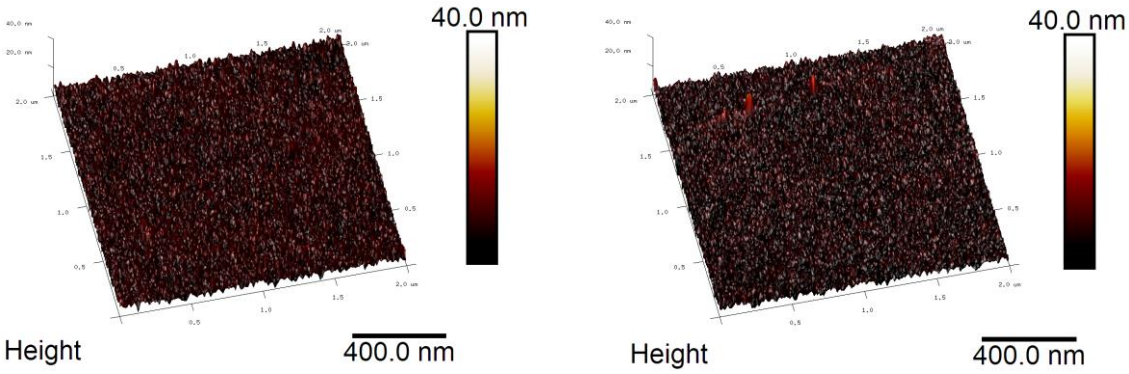


a b

**Figure 31.** The 3D-recovery of surface topography for samples #2 (a) and #3 (b). Area of investigation is 2x2 μm.

**Table 6.** The RMS roughess value for samples.

| Sample number | RMS roughness (nm) | |
|---|---|---|
| | 30x30 μm area | 2x2 μm area |
| 1 | 2.6 | 3.7 |
| 2 | 8.9 | 1.6 |
| 3 | 1.6 | 1.6 |
| 4 | 15.8 | 7.8 |
| 5 | 41.7 | 11 |
| 6 | 110 | 3 |
| 7 | 9.1 | 7.5 |
| 8 | 22.5 | 7.5 |
| 9 | 3.2 | 3.8 |
| 10 | 12 | 8.2 |
| 11 | 4.3 | 4.1 |
| 12 | 48.9 | 3.8 |
| Si-Ni 1 | 1.3 | 0.8 |
| Si-Ni 2 | 2.2 | 0.4 |
| Si-Ni 3 | 10.6 | 0.7 |

### 5.2. Additional studies

Unfortunatelly, Ni and Si material were not distinguiched by KPFM method. Contrast was not detected in study by MFM (Figure 35). There is an assumption that it can be associated with a uniform coating surface of the Ni particles. Since these investigation methods are comparative they can not permit qualitative study in this case. However, some magnetic contrast is visible on the sample #12 (Figure 36). Presumably the nickel particles are laid unevenly in this area during etching. This effect requires further study.

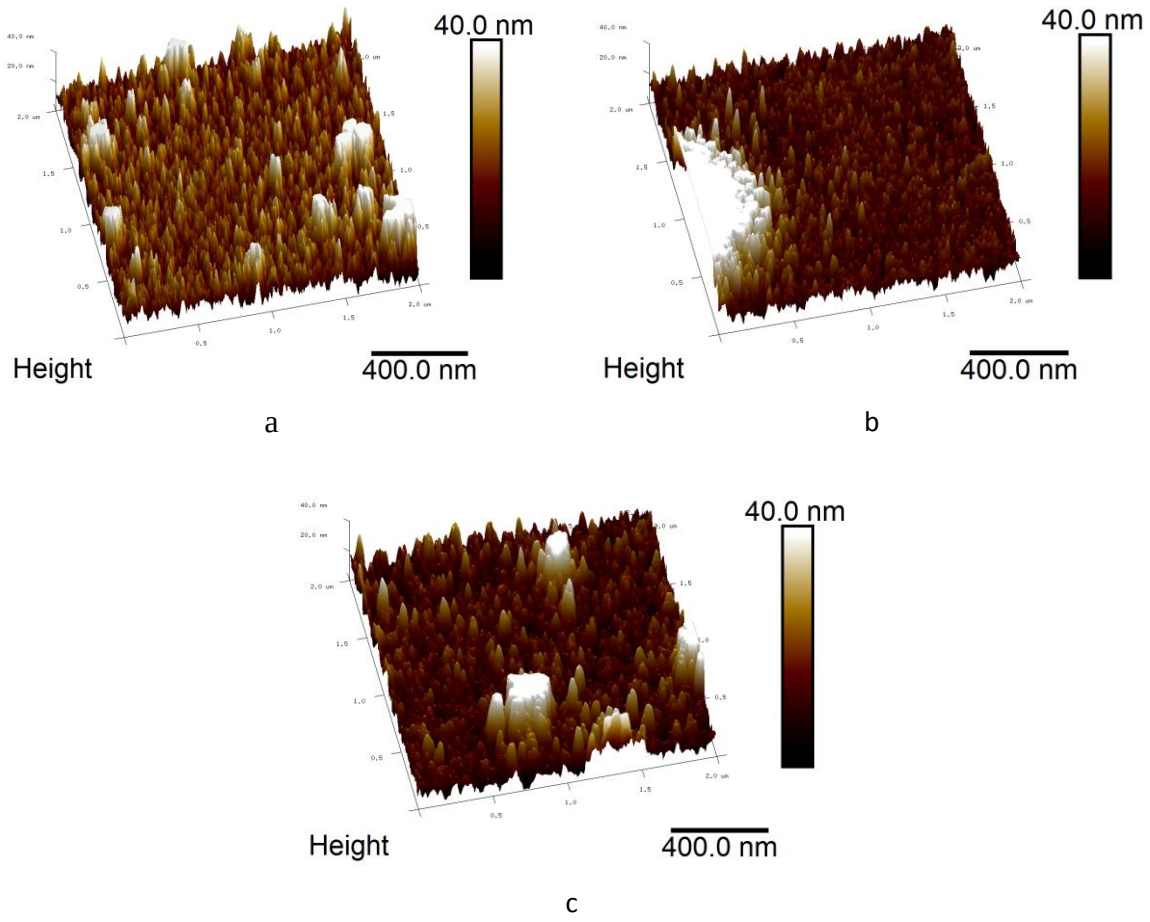


**Figure 32.** The 3D-recovery of surface topography for samples #4 (a), #5 (b) and #6 (c). Area of investigation is 2x2 um.

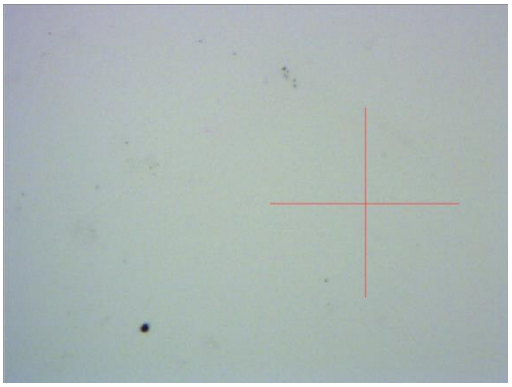

#1

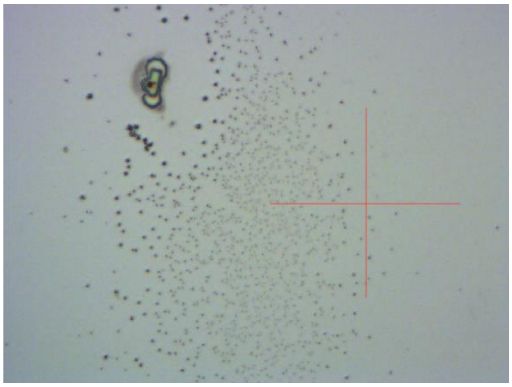

#2

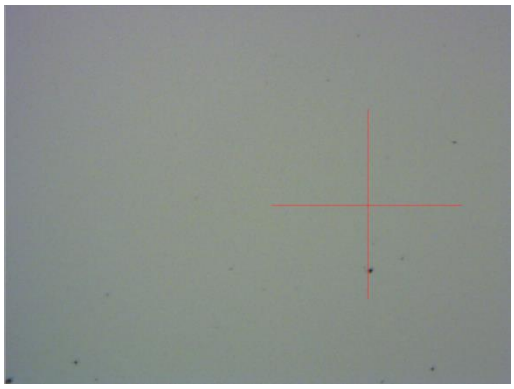

#3

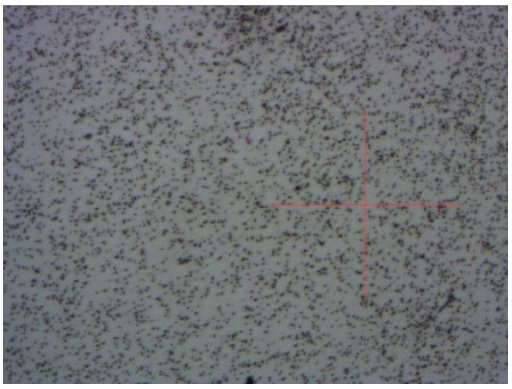

#4

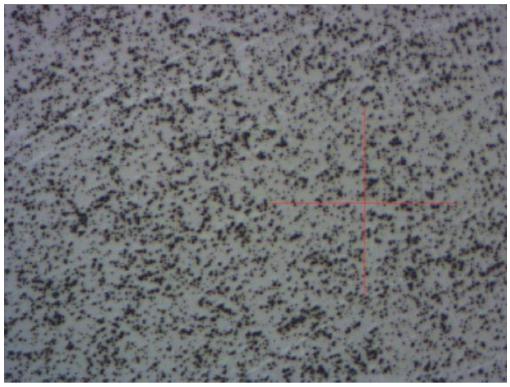

#5

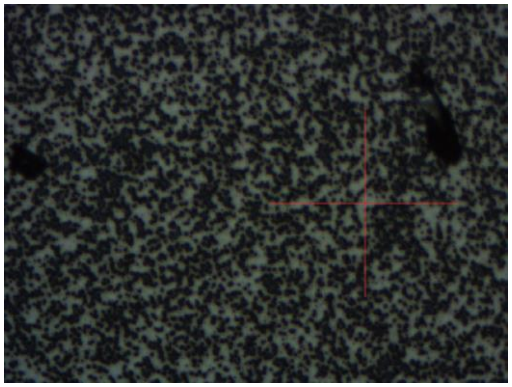

#6

**Figure 33.** Images obtained by optical microscope of samples. Investigation area is 370x500 μm.

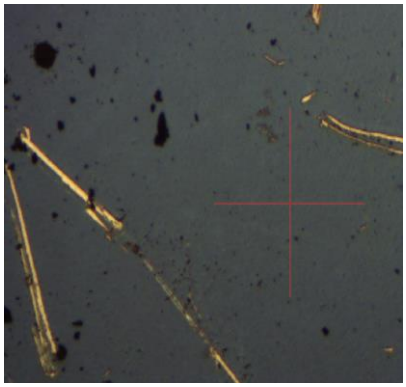

#7

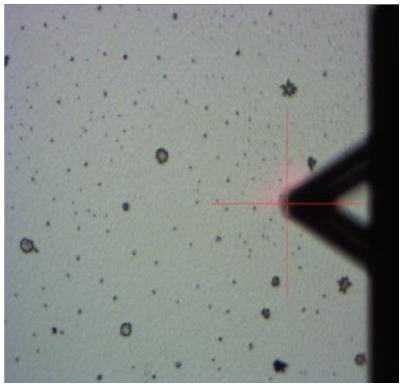

#8

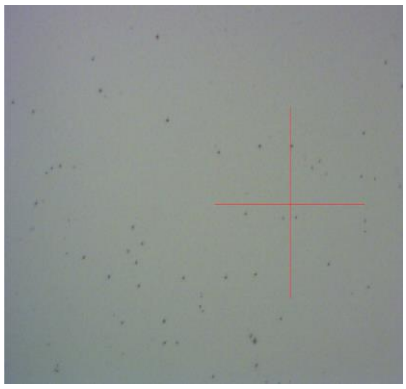

#9

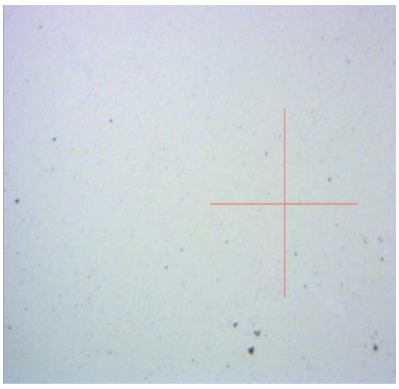

#10

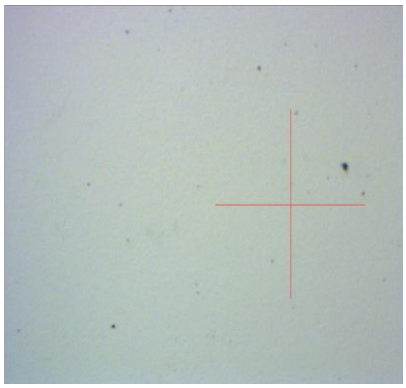

#11

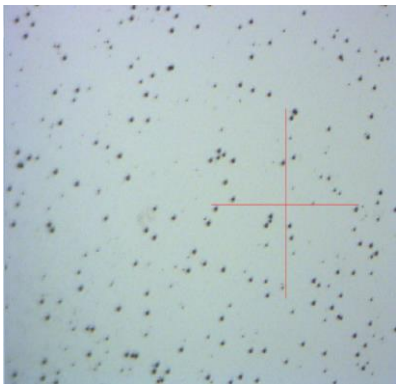

#12

**Figure 34.** Images obtained by optical microscope of samples. Investigation area is 370x500 μm.

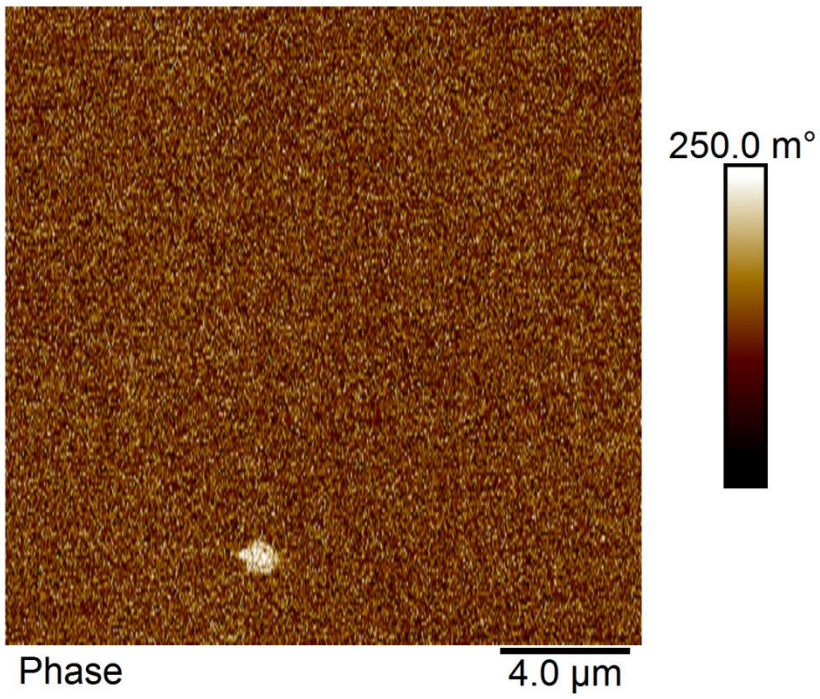


**Figure 35.** MFM signal from sample #9. Small infomagenity is caused by lifting up the tip, while surface seems flat at MFM.

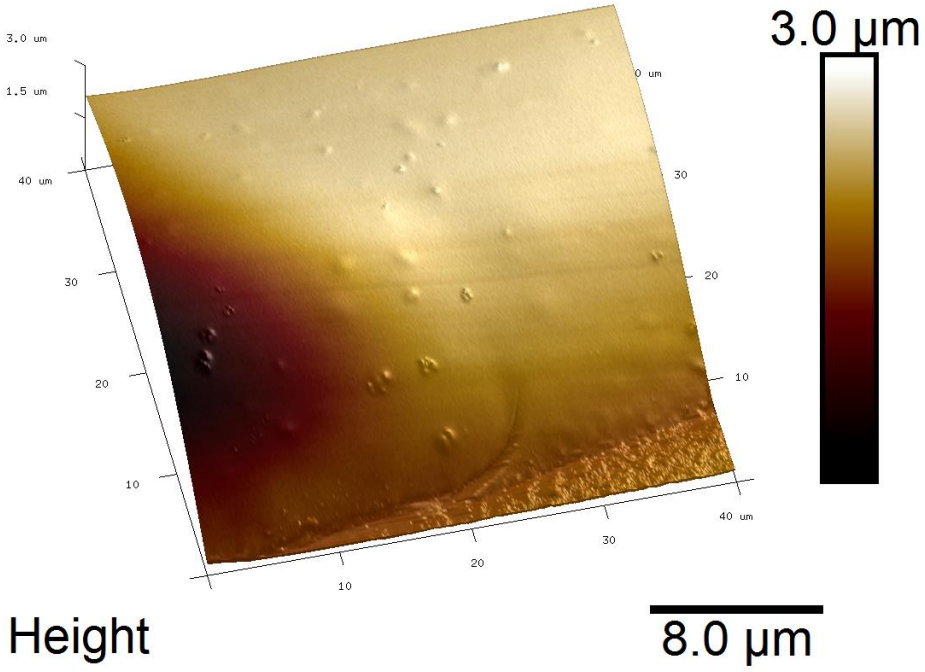


**Figure 36.** MFM signal sample #12. 3D topography with magnetic phase channel data ”skin” put on it. Left part show magnetic signal.

Works [71, 73] describe a method of cross-section study of porous silicon. In these works a boundary between the porous silicon and the substrate width of 3 microns was noticed. The sample #9 was split and its cross-section was studied by AFM (Figure 37). It

was expected to distinguish the border between P-Si and Si. However, this border was not observed, but the elevation can be seen at the right and left side of the sample. It may be connected with the porous region. Meanwhile KPFM line is visible and not correlated with the topography. Thus MFM signal at that location does not have any changes. This may be due to the composition in the pores: an oxide, hydroxide, penetrated through the pores, or nickel is deposited more dense. In this case, the MFM signal can not show contrast, because part of material surface or the entire surface is nonmagnetic.

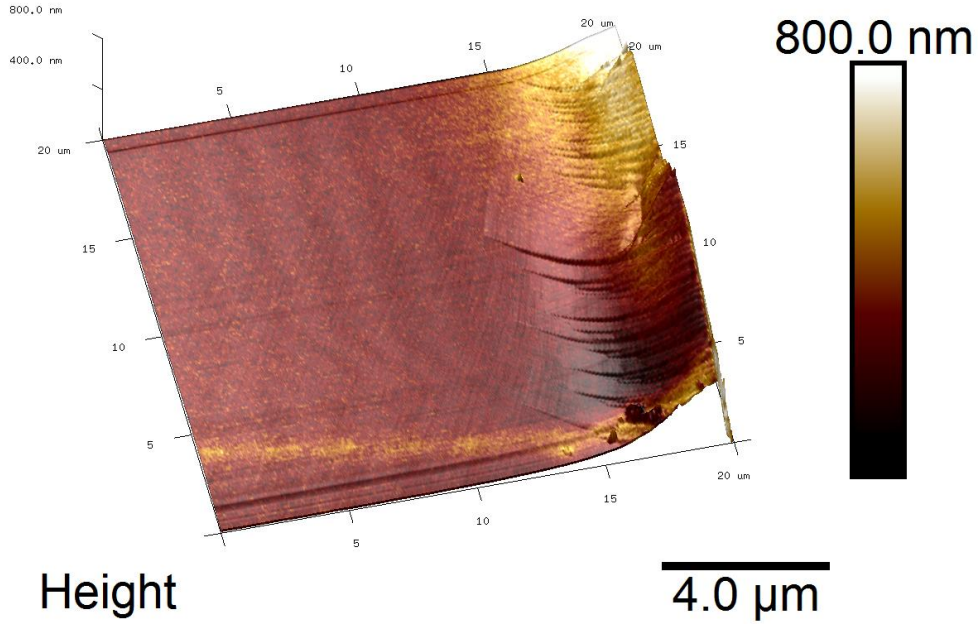


**Figure 37.** KPFM Cross-section scan data for sample #9 with Lift distance = 150 nm. Surface potential color skin was put on surface 3D topography. Rough edge of the sample is seen on the right side. Contrast is seen both on the right side and as the straight white line down left. This line did not appear on Magnetic phase image at same area afterwards.

A theory exists that photoluminescence in silicon under UV illumination induces changing the energy surface. These changes should be possible to observe by the mode KPFM. However, the contrast is not observed during our investigation of sample by this method.

The surface conductivity of samples was also investigated by multimeter. The study showed that the samples were not conducted. This can be induced by the fact that the surface is not completely covered with nickel particles, i.e. the percolation threshold is not reached.

## Conclusions

1) According to the AFM data, differences in topography were noticed. These differences allow to link the treatment effect and the surface because periodical changes of roughness were noticed.

2) The height of a silicon monolayer was measured to be 215 picometers, in good agreement with table data. After the treatment (etching) all monolayers disappeared (dissolved) and surface became rough.

3) Differences in sample morphology appear in roughness. This indicates pores (and particles). In contrast to the expectations on AFM images appeared mainly micropores.

4) The values of roughness are obtained for 2 and 30 micron areas. Areas of investigation seemed inhomogeneous, but roughness of etched samples increases.

5) Particles are observed also on optical microscope images. Their density and size correspond to the treatment condition. Particles amount and their size increase with the duration of ething process. Probably, small subnanometer particles of Ni also fill up the micropores, which affected roughness to decrease in series.

6) KPFM does not show differences in surface workfunction for specific areas of one sample, same as for particles compared to the surface. Probably it can be explained by the fact, that surface pores are filled with nano-size Ni particles and pores are not distinguished by KPFM.

7) Phase contrast was not detected by MFM to clarify the magnetic domain nature of surface particles. However, some magnetic contrast is visible on the sample #12. It can also be explained by even filling of pores by Ni particles.

8) Cross-section of sample #9 shows the elevation at the right and left sides. It may be due to ending of the porous region.

9) KPFM image of cross-section revealed the contrast line, which is not correlated with topography. MFM did not display any changes at that zone measured again. This area can be filled by Ni particles with different concentration.

10) Sample study by KPFM under UF illuminescence does not show shift in phase data. This negotiates the assumption about the micropore size. However, if their real size is in the border region, no influence should be observed.

11) The investigation of the surface conductivity by multimeter showed that the samples surface is not conductive. Thus if surface pores are filled by Ni nanopericles, they are not electrically connected to each other, i.e. percolation threshold is not reached.

**Summary**

In this work, porous silicon with deposited nickel particles was investigated by different AFM modes: Peakforce, tapping, MFM and KPFM. A technique of AFM study was developed for the purposes to investigate these samples, since earlier in literature samples were studied only by Tapping mode. The topography measurements were conducted using a Bruker Multimode 8 microscope in PeakForce mode.

The main highlights of this work are as follows:

1) Particles are detected on the surface of samples by the optical microscope and the AFM device. Firstly, amount of particles rises in the series. After that, size of the particles increases with duration of electrochemical deposition of Ni.

2) Size of the pores is observed to be between 1 and 10 nm. No deep pores were observed by AFM, but only rough surface. According to "border" nature of the size, no photoluminescence effect was noticed.

3) Research by KPFM and MFM methods mainly did not show any contrast. This may indicate a non-conducting structure or uniform surface coating. Thus we can conclude, that surface has been filled by nanometer sized Ni particles. Partially they have grown to ~ 1μm large particles on surface. Although KPFM and MFM methods are comparative, so in above mentioned cases it is not possible to observe any contrast.

This master's thesis contains figures and tables of data to demonstrate the occurring phenomena. Final conclusions should be verified by other reliable method, e.g. RAMAN and TEM.

The main drawback of the porous structure measurement by AFM is that the probe can be larger than the size of examined pores. In this case, it is impossible to fully describe the morphology. It is possible to see only the top of the pore, if it is mainly micropores like in our samples.

On basis of our result and literature review further research direction can be named to answer the open question. It is needed:

1) to study the samples by SEM on their cross-section to determine an etching depth;

2) to find the etching thickness (depth) by ellipsometry by refractive index data;

3) to compare photoluminescence of P-Si and P-Si modified by Ni particles in details;

4) to implement Raman spectroscopy to obtain information about compound on the P-Si surface: are they Ni oxides, hydroxides or $SiO_2$;

5) to investigate a signal from Ni particles deposited on P-Si by SQUID magnetometer. It is expected to be possible to calculate the amount of Ni by magnetic intensity of signal and areas under the magnetization curves. Even Ni particles sizes can be calculated as Ni nanoparticles must demonstrate paramagnetism, ferromagnetism or superparamagnetism depending on their size.

## References


[1] Zhang, G. X. 2005. Porous Silicon: Morphology and Formation Mechanisms. *Modern Aspects of Electrochemistry*, Number 39, pp. 65-133. New-York: Springer.

[2] Sailor, M. J. 2012. Porous Silicon in Practice: Preparation, Characterization and Applications. 1st ed. Wiley-VCH Verlag GmbH & Co. KGaA.

[3] Elisabet Xifré Pérez 2007. Design, fabrication and characterization of porous silicon multilayer optical devices. Ph.D. thesis. Universitat Rovira I Virgili, Departament d'Enginyeria Electrònica, Elèctrica i Automàtica.

[4] Moshnikov, V.A. & Terukov, E.I. 2011. Basics of hydrogen energy. 2nd ed. Saint-Petersburg: Saint-Petersburg Electrotechnical University "LETI". (in Russian)

[5] Föll, H. & Christophersen, M. & Carstensen, J. & Hasse, G. 2002. Formation and application of porous silicon. *Materials Science and Engineering*. R 280, pp. 1–49.

[6] Harraza, F.A. & Ismaila, A.A. & Bouzid, H. & Al-Sayari, S.A. & Al-Hajry, A. & Al-Assiri, M.S. 2014. A capacitive chemical sensor based on porous silicon for detection of polar and non-polar organic solvents. *Applied Surface Science*, v. 307, pp. 704-711.

[7] Saakshi Dhanekar & Swati Jain. 2013. Porous silicon biosensor: current status. *Biosensors and Bioelectronics*. v. 41, pp. 54–64.

[8] Baratto, C. & Comini, E. & Faglia, G. & Sberveglieri, G. & Di Francia, G. & De Filippo, F. & La Ferrara, V. & Quercia, L. & Lancellotti, L. 2000. Gas detection with a porous silicon based sensor. *Sensors and Actuators.* B 65, pp. 257–259.

[9] RoyChaudhuri, C. 2015. A review on porous silicon based electrochemical biosensors: Beyond surface area enhancement factor. *Sensors and Actuators* v. B 210, pp. 310–323.

[10] Harraz, Farid A. 2014. Porous silicon chemical sensors and biosensors: a review. *Sensors and Actuators.* v. B 202, pp. 897–912.

[11] Anglin, Emily J. & Lingyun Cheng & Freeman, William R. & Sailor, Michael J. 2008. Porous silicon in drug delivery devices and materials. *Advanced Drug Delivery Reviews*. v. 60, pp. 1266–1277.

[12] Yuzova, V.A. & Puzir, A. P. 2008. Introduction of diamond soot of detonation synthesis in the channels of porous silicon. *Letters to JTF*. v. 34, pp.34–38. *(in Russian)*

[13] Eftekhari, A. 2008. Nanostructured materials in electrochemistry. WILEY-VCH Verlag GmbH & Co. KGaA, Weinheim.

[14] Di Bari, G. 1994. Nickel plating. Surface Engineering. v. 5, p. 201.

[15] Turner, D. R. 1958 *J. Electrochem. Soc., v. 105, p.* 402.

[16] Uhlir, A. 1956 Jr., *The Bell System TechnicalJournal,* March, 333.

[17] Memming, R. & Schwandt, G. 1966. *Surf. Sci. v.* 4, p. 109.

[18] Meek, R. L. 1971. *J. Electrochem. SocUH.* 437.

[19] Theunissen, M. J. J. 1972. J: *Electrochem. Soc, v.* 119, p. 351.

[20] Arita, Y. & Sunahama, Y. 1977 *Electrochem. Soc, v.* 124, p. 285.

[21] Watanabe, Y. & Arita, Y. & Yokoyama, T. & Lgarashi, Y. 1975. *J. Electrochem. Soc, v.* 122, p. 1315.

[22] Bomchil, G. & Herino, R. & Barla, K. & Pfister, J. C. 1983. *J. Electrochem.* Soc., v. 130, p. 1611.

[23] Uganami, T. & Seki, M., 1978. *J. Electrochem. Soc., v. 125,* p.1339.

[24] Labunov, V. & Baranov, I. & Bondarenko, V. 1979. *Thin Solid Film, v.* 64, p. 479.

[25] Beale, M. I. J. & Benjamin, J. D. & Uren, M. J. & Chew, N. G. & Cullis, A. G. 1985. *J. Crystal Growth, v.* 73, p. 622.

[26] Chuang, S. F. & Collins, S. D. & Smith, R. L. 1989. *Appl. Phy. Lett., v.* 55(7), 14 August, p. 675.

[27] Smith, R. L. & Collins, S. D. 1992. *J. Appl. Phy. v.* 71(8), 15 April, Rl.

[28] Smith, R. L. & Chuang, S. F. & Collins, S. D. 1988. *J. Electronic Materials, v.* 17, p.228.

[29] Unagami, T. 1980. *J. Electrochem. Sac., v.* 127**,** p. 476.

[30] Parkhutik, V. P. & Glinenko, L. K. & Labunov, V.A. 1983. *Surface Technology, v.* 20, p. 265.

[31] Zhang, X. G. & Collins, S. D. & Smith, R. L. 1989. *J. Electrochem.* Soc., v. 136, p. 1561.

[32] Zhang, X.G. 1991. *J. Electrochem. Soc, v.* 138, p. 3750.

[33] Carstensen, J. & Christophersen, M. & Foil, H. 2000. *Materials Science and Engineering* B69-70, p. 23.

[34] Jaguiro, P. & La Monica, S. & Lazarouk, S. & Ferrari, A. 1997. *Electrochemical Society Proceedings, v.* 91-1, p. 296.

[35] Zhang, X. G. 2001. *Electrochemistry of Silicon and Its Oxide,* Kluwer Academic, New York.

[36] Burrows, V. A. & Chabal, Y. J. & Higashi, G. S. & Raghavachari, K. & Christman, S. B. 1988. *Appl. Phys. Lett., v.* 53(11), p. 998.

[37] Gronet, C. M. & Lewis, N. S. & Cogan, G. & Gibbons, J. 1983. *Proc Natl. Acad. Sci.* USA, v. 80, p. 1152.

[38] Cobianu, C. & Savaniu, C. & Buiu, O. & Dascalu, D. & Zaharescu, M. & Parlog, C. & van den Berg, A. & Pecz, B. 1997. Tin dioxide sol – gel derived thin films deposited on porous silicon. *Sensors and Actuators.* v. B 43, pp. 114 – 120.

[39] Macherzynskia, M. & Milczareka, G. & Mamykina, S. & Romanyuka, V. & Kasuya, A. 2010. Electrochemical preparation of photosensitive porous n-type Si electrodes, modified with Pt and Ru nanoparticles. *Electrochimica Acta*. v. 55, pp. 4395–4401.

[40] Yuzova, V.A., Levitsky, A.A. Harlashin, P.A. 2011. Development Technology of Creation and Research Porous Silicon. *Journal of Siberian Federal University. Engineering & Technologies*. v. 4(1), pp. 92-112.

[41] Langa, S. & Carstensen, J. & Christophersen, M. & Foll, H. & I.M. Tiginyanu, I. M. 2005. The Way to Uniformity in Porous III–V Compounds via Self-Organization and Lithography Patterning. Ordered Porous Nanostructures and Applications. Springer Science + Business Media, pp. 57 – 87.

[42] Takizawa, T. & Arai, Sh. & Nakahara, M. 1994. Fabrication of vertical and uniform-size porous InP structure by electrochemical anodization. Japan. *J. Appl. Phys.* v. 54(2), pp. L643–L645.

[43] Antropov, I.M. & Demidovitch, G.B. & Kozlov, S.N. 2011. Adsorption sensitivity of nanocomposite "porous silicon - nickel" to methane. *Technical Physics Letters.* v. 37 (5), pp. 43 – 48.

[44] Moshnikov, V.A. & Gracheva, I.E. & Lenshin, A.S. & Spivak, Y.M. & Anchkov, M.G. & Kuznetsov, V.V. & Olchowik, J.M. 2012. Porous silicon with embedded metal oxides for gas sensing applications. *Journal of Non-Crystalline Solids*. v. 358, pp. 590–595.

[45] Kononova, I.E. & Moshnikov, V.A. & Olchowik, G. & Len'shin, A.S. & Gareev, K.G. & Soboleva, E.A. & Kuznetsov, V.V. & Olchowik, J.M. 2014. The preparation and properties of "porous silicon-nickel ferrite" nanoheterocomposites for gas detectors. *J Sol-Gel Sci Technol.* DOI 10.1007/s10971-014-3353-1.

[46] Amdouni, A & Rahmani, M. & Zaïbi, M.-A. & Oueslati, M. 2015. Enhancement of porous silicon photoluminescence by electroless deposition of nickel. *Journal of Luminescence.* v. 157, pp. 93–97.

[47] Zhang, Y.Q. & Xia, X.H. & Wang, X.L. & Mai, Y.J. & Shi, S.J. & Tang, Y.Y. & Gu, C.G. & Tu, J.P. 2012. Three-dimensional porous nano-Ni supported silicon composite film for high-performance lithium-ion batteries. *Journal of Power Sources*. v. 213, pp. 106-111.

[48] Qian, X. & Hang, T. & Nara, H. & Yokoshima, T. & Li, M. & Osaka, T. 2014. Electrodeposited three-dimensional porous Si-O-C/Ni thick film as high performance anode for lithium-ion batteries. *Journal of Power Sources.* v. 272, pp. 794-799.

[49] Wang, X. & Sun, L. & Hu, X. & Susantyoko, R.A. & Zhang, Q. 2015. Ni-Si nanosheet network as high performance anode for Li ion batteries. *Journal of Power Sources.* v. 280, pp. 393-396.

[50] Eskhult, J. 2007. Electrochemical deposition of nanostructured metal/metal-oxide coatings. Doctoral dissertation. Uppsala University. Department of Materials Chemistry.

[51] Gavrilov, S.A. & Belov, A.N. & Zheleznyakova, A.V. 2011. Lectures "Low-temperature processes in the technology of nanoelectronics and nanosystems". Moscow: MIET.

[52] Maximov, A.I. & Moshnikov, V.A. & Tairov, Yu.M. & Shilova, O.A. 2007. Basics of sol-gel technology of nanocomposites. Saint-Petersburg, Russia: Elmor.

[53] Brinker, C. J. & Scherer, G. W. 1990. Sol-Gel Science. The Physics and Chemistry of Sol-Gel Processing. San Diego: Academic Press.

[54] Shklovskii, B.I. & Efros, A.L. 1979. Electronic properties of doped semiconductors. Moscow: Nauka.

[55] Pomogailo, A.D. & Rosenberg, A.S. & Uflyand, I.E. 2000. Metal nanoparticles in polymers. Moscow: Chemistry.

[56]Feynman, R.P. 1960. There's Plenty of Room at the Bottom. *Caltech Engineering and Science*, V. 23:5, pp 22-36.

[57] Young, R. 1971. Phys.Today, v.24.p.42.

[58] Jin-Feng Jia & Wei-Sheng Yang & Qi-Kun Xue. 2006. Scanning Tunneling Microscopy. Handbook of Microscopy for nanotechnology. Springer. pp. 55-112

[59] Franz J. Giessibl & Calvin F. Quate. 2006. Exploring the nanoworld with atomic force microscopy. Physics Today.

[60] C. Julian Chen. 2008. Introduction to Scanning Tunneling Microscopy. Second Edition Department of Applied Physics and Applied Mathematics Columbia University, New York Copyright, Oxford University Press.

[61] Holger Schönherr & G. Julius Vancso. 2010. Atomic Force Microscopy in Practice, Scanning Force Microscopy of Polymers, Springer Laboratory**.**

[62] Mironov, V. 2004. Fundamentals of Scanning Probe Microscopy, N.Novgorod, (in Russian).

[63] Application Note #128 Quantitative Mechanical Property Mapping at the Nanoscale with PeakForce QNM 2012 Bruker Corporation.

[64] KP Technology Ltd., Burn Street, Wick, Caithness, Scotland, KW1 5EH. [Accessed 25.04.2015] Available at http://www.kelvinprobe.info/

[65] Nonnenmacher, M. & O'Boyle,P. & Wickramasinghe,H.K. 1991. Kelvin probe force microscopy, Appl. Phys. Lett. 58 (25): 2921.

[66] Sadewasser, S. & Glatzel, Th. 2011. Kelvin Probe Force Microscopy: Measuring and Compensating Electrostatic Forces, Springer Series in Surface Sciences, volume 48.

[67] Titkov, A.N. & Girard, P. 2006. Electrostatic Force and Force Gradient Microscopy: Principles, Points of Interest and Application to Characterisation of Semiconductor Materials and Devices, Applied Scanning Probe Methods II, NanoScience and Technology.

[68] Wilhelm Melitz & Jian Shen & Andrew C. Kummel & Sangyeo Lee. 2011. Kelvin probe force microscopy and its application. *Surface Science Reports*. v. 66, pp. 1–27.

[69] Yaminsky, I.V. & Tishin, A.M. Magnetic force microscopy. *Russian Chemical Review*. v. s68(3), pp. 165-170

[70] Bruker AFM probes. [accessed 30.04.2015] Available at http://www.brukerafmprobes.com

[71] J. Martı´n-Palma & Vicente Torres-Costa & Leigh Canham. 2014. Microscopy of Porous Silicon. Handbook of Porous Silicon Springer International Publishing Switzerland.

[72] Hasan A. Hadi1 & Raid A. Ismail & Nadir F. Habubi1. 2013. Fabrication and characterization of porous silicon layer prepared by photo-electrochemical etching in $CH_3OH$:HF solution. *International Letters of Chemistry, Physics and Astronomy. V. 8, pp 29-36.*

[73] Granitzer, P. & Rumpf, K. & Poelt, P. & Plank, H. & Albu, M. 2010. Ferromagnetic nanostructure arrays self-assembled in mesoporous silicon. *Journal of Physics: Conference Series* v. 200.